Upscaling of a sulphur dioxide depolarized electrolyzer

M P Coetzee

20249705

Dissertation submitted in partial fulfilment of the requirements for the degree Master of Engineering at the Potchefstroom Campus of the North-West University

Supervisor: Professor J. Markgraaff

February 2012

ACKNOWLEDGEMENTS

I would firstly like to thank my Supervisor, Prof. J Markgraaff for his guidance over these past two years, it has truly been a privilege to have such a wise and insightful study leader. I would also like to thank Mr. A. Kruger and Prof. H. Krieg for their help on the chemistry aspects of the project.

Thank you to my friends and family, especially my parents for their continued support over the period of my studies, I am truly indebted to you.

And lastly, to the most important contributor to my success, God. Thank you for giving me the strength, wisdom, patience and insight to complete this project.

Thank you.

ABSTRACT

In the last couple of years there has been a great need for finding alternative, cleaner burning fuel sources. This search has led to the development of various hydrogen technologies. The reason for this is that when burnt, hydrogen gas only forms water and oxygen as products. One of the methods used in the production of hydrogen gas is that of the electrolysis of sulphur dioxide which is facilitated by a sulphur dioxide depolarized electrolyzer. The electrolysis of sulphur dioxide has the advantage of requiring lower cell voltages in the electrolysis process when compared to the electrolysis of water.

This type of electrolyzer unfortunately suffers from low hydrogen gas production volumes. It was thought that by linearly increasing the reactions active area of the electrolyzer, the production volumes can be increased. A linearly upscaled 100cm^2 cell was designed by using computer aided design software, such as SolidWorks, Cambridge Engineering Selector, EES and ANSYS. The cell was then constructed and tested to determine the effects of linearly upscaling. The results of the 100cm^2 cell were compared to the results of a similar 25cm^2 cell and results obtained from the literature. The 100cm^2 cell exhibited very poor performance when compared to the other cells. The 100cm^2 cell showed lower hydrogen production volumes at higher energy inputs than the 25cm^2 cell and an 86cm^2 stack assembly. It was concluded that creating stack assemblies with cells with smaller active areas would be much more efficient than linearly upscaling the active area of the cells.

Keywords: Sulphur dioxide; Electrolysis; Hydrogen production; Proton exchange membrane; Bipolar plates, Linear upscaling

OPSOMMING

In die afgelope paar jaar is daar meer druk op die wetenskaplike gemeenskap geplaas om skoner brandende brandstowwe te vind. Hierdie soektog het gelei tot die uitbreiding van waterstof tegnologie. Die rede hiervoor is dat wanneer waterstof ontbrand, slegs water en suurstof gevorm word. Waterstof word deur verskeie prosesse geproduseer, insluitend die elektrolise van swael dioksied en water d.m.v. die swael dioksied gedepolariseerde elektroliseerder. Die voordeel van die elektrolise van swael dioksied is die laer spanning wat nodig is tydens die elektrolise proses in vergelyking met die elektrolise van water.

Die elektroliseerder het tans die nadeel van lae waterstof gasproduksie tempo's. Daar bestaan 'n moontlikheid dat lineêre opskaling van die elektroliseerder se aktiewe area tot hoër produksie tempo's sal lei. 'n Liniêr opgeskaalde 100cm^2 elektroliseerder is ontwerp deur van rekenaar gesteunde ontwerp programmatuur soos SolidWorks, Cambridge Engineering Selector, EES en ANSYS gebruik te maak. Die elektroliseerder is toe gebou en getoets om die gevolge van lineêre opskaling te evalueer. Toetse is op die 100cm^2 sel en 'n soortgelyke 25cm^2 sel uitgevoer en die resultate is vergelyk met resultate uit die literatuur. Die resultate het getoon dat die 100cm^2 sel baie sleg gevaar het. Die 100cm^2 sel het laer waterstof produksie tempo's by hoër energie insette as die 25cm^2 sel en 'n 86cm^2 stapel-samestelling getoon. Daar is vasgestel dat meer selle met kleiner aktiewe areas meer effektief sal wees as om een sel liniêr op te skaal.

Sleutelwoorde: Swael dioksied; Elektrolise; Waterstof produksie; Proton ruil membraan, Bipolêre plate, Lineêre opskaling

TABLE OF CONTENTS

LIST OF FIGURES

LIST OF TABLES

LIST OF ABBREVIATIONS

Al	Aluminium
CAD	Computer Aided Design
CES	Cambridge engineering selector
EES	Engineering Equation Solver
GDL	Gas Diffusion Layer
GES	Giner Electrochemical Systems
GHG	Green House Gas
HyS	Hybrid Sulphur
MEA	Membrane Electrode Assembly
MES	Membraan Elektrode Samestelling
MSDS	Material Safety Data sheet
NPT	National Pipe Thread
NWU	North-West University
PEM	Proton Exchange Membrane
PES	Proton Energy Systems
PFA	Perfluoroalkoxyethylene
PTFE	Polytetrafluoroethylene
RTV	Room Temperature Vulcanizing
SDE	Sulphur Dioxide Depolarized Electrolyzer
SEM	Scanning Electron Microscopy
SI	Sulphur-Iodine
SS	Stainless Steel
ZAR	South Africa Rand

1 INTRODUCTION

1.1 Background

We live in a world where there is a growing concern over our personal well being, as well as that of our planet. Our main source of energy comes from the burning of fossil fuels, natural gases and due to the great number of automobiles, petroleum [1]. Below is a figure illustrating the usage of these energy sources.

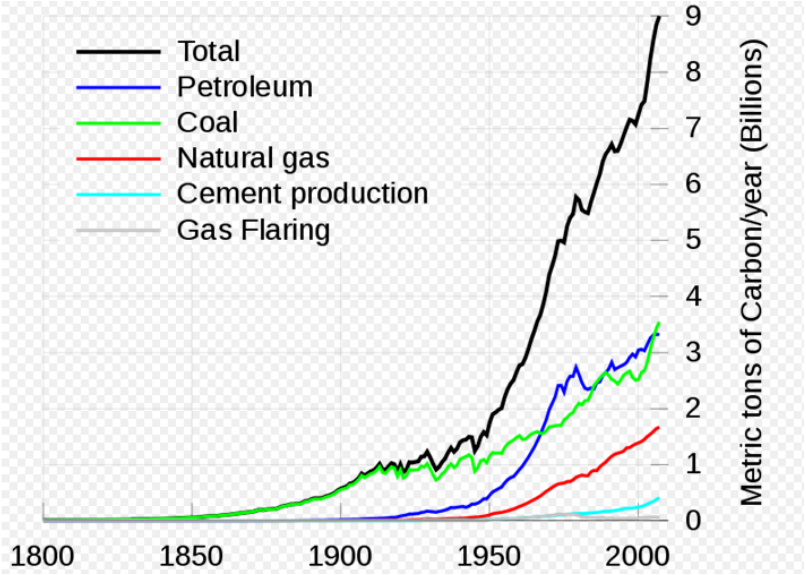

Figure 1: Illustration of the production of CO_2 during the burning of various fuels

The burning of these fuels lead to the formation of green house gases (GHG's). These GHG's in turn leads to global warming and climate changes. A great deal of research is being done on finding alternative, cleaner burning energy sources. The search for these cleaner fuels has led to various hydrogen technologies being investigated.

Hydrogen is the most abundant element in the universe and the tenth most abundant element on the surface of the planet [2]. This already eliminates the problem of shortage of raw materials. Hydrogen also has the highest energy per mass ratio of any conventional fuel [3] and when combustion of hydrogen gas (H_2) occurs, the only products formed are water (H_2O) and oxygen (O_2). Unfortunately hydrogen is almost always found combined with other chemical species. In order to benefit from this great energy carrier, the hydrogen

containing substances have to be split to form hydrogen gas. This can be done by electrolysis and a number of other electrical and/or thermochemical processes. Some of the most promising electrolysis processes are the sulphur based cycles like the Sulphur-Iodine (SI) cycle and the Hybrid Sulphur (HyS) cycle.

The hydrogen gas that is produced by these cycles can be used by a fuel cell to produce electricity or may be combusted in an internal combustion engine. The long term goal of hydrogen production is to produce hydrogen gas to power automobiles and to a certain degree produce electricity for households or industrial applications to alleviate the massive degree of carbon dioxide emissions from the burning of fossil fuels or natural gasses.

1.1.1 Hydrogen production via electrolysis

There is a great number of electrolysis processes used for the production of hydrogen gas with water electrolysis being the most conventional method. Electrolysis is a process whereby a direct electric current (DC) is passed through an electrolyte causing chemical reactions to take place [4]. The electrolysis process is facilitated by an electrolyzer which is comprised of an electrolyte and one positive (anode) and one negative electrode (cathode). A simplified schematic of such an electrolytic cell is illustrated in Figure 2 . In the case of water electrolysis, oxygen gas will form at the anode whilst hydrogen gas is produced at the cathode.

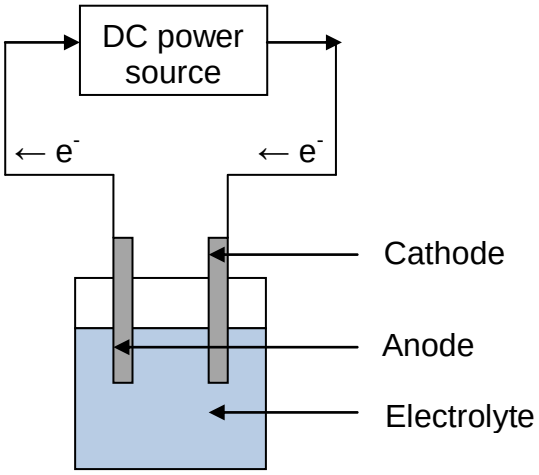

Figure 2: Simplified schematic of an electrolytic cell

The focus for new research has shifted towards the electrolysis of sulphur dioxide (SO_2) as with the sulphur based cycles. The sulphur based cycles consists of the thermal decomposition of sulphuric acid (H_2SO_4) to form sulphur dioxide and oxygen, the sulphur dioxide is then used along with water in an electrolyzer to form hydrogen gas. The electrolysis steps in these cycles are facilitated by a Proton Exchange Membrane (PEM).

1.1.2 Hybrid sulphur (HyS) cycle

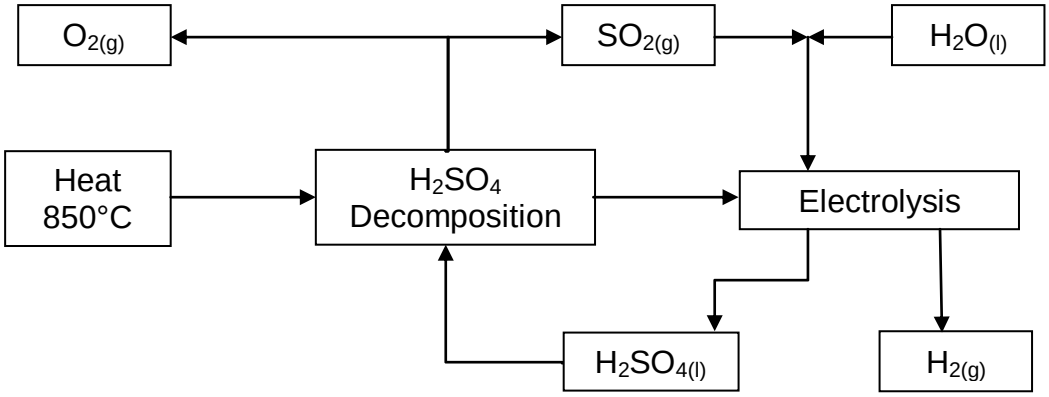

Figure 3: Schematic illustration of the hybrid sulphur cycle modified after P. Sivasubramanian *et al.* (2007)

The hybrid sulphur cycle, also known as the Westinghouse cycle, which was developed in the 1970's, is a two step process consisting of an electrolysis step and a thermochemical step.

The first step in this cycle is the thermal decomposition of sulphuric acid into sulphur trioxide and steam. This step is done at around 850°C. The sulphur trioxide is then further decomposed into sulphur dioxide and oxygen. The sulphur dioxide is then used in the electrolysis step with water to form sulphuric acid and hydrogen gas in a Sulphur Dioxide Depolarized Electrolyzer (SDE) [5].

The electrolysis step is done at low temperatures in the range of 80°C - 100°C which improves the reaction kinetics within the electrolyzer. The elevated temperature is usually supplied by a heating pad. The main components of the SDE are the bipolar plates containing flow fields and the PEM which is typically fused with a gas diffusion layer (GDL) containing a catalyst for the

chemical reactions. The PEM along with the gas diffusion layers and catalyst layers are known as the Membrane Electrode Assembly (MEA, Figure 4).

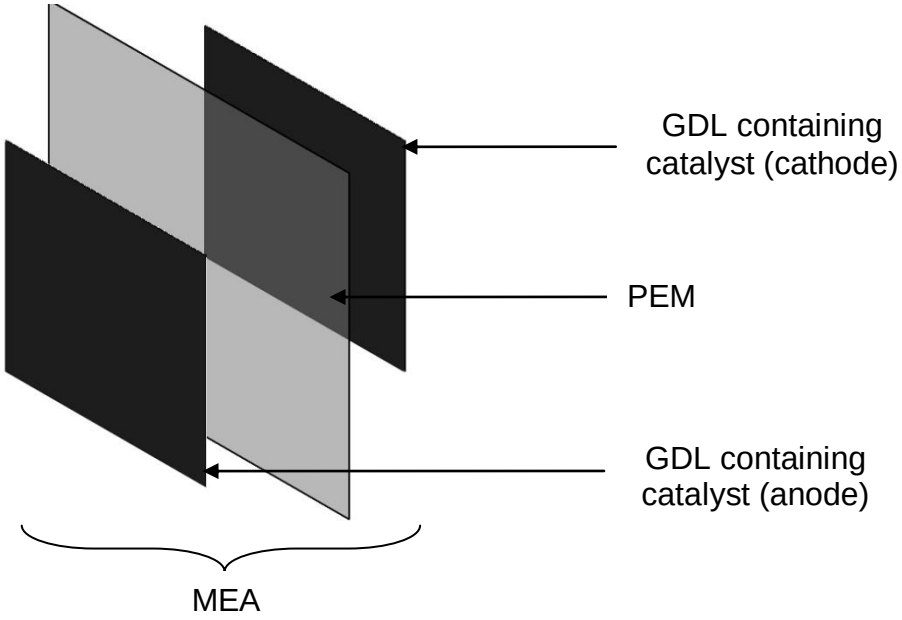

Figure 4: Exploded view of MEA consisting of the PEM and GDL's

The hybrid sulphur cycle is a popular choice for new research because it requires a lower electrode potential (cell voltage) for the electrolysis step [6] and makes use of relatively inexpensive chemicals [7]. Direct water electrolysis uses a theoretical cell voltage of 1.23V whilst the hybrid sulphur cycle only needs a theoretical cell voltage of 0.17V, depending on the operating conditions [6]. The expected actual cell voltage is in the range of 0.5-0.6V [8]. A lower electrode potential is required because the sulphur dioxide depolarizes the anode [9].

The chemical stock needed for the HyS cycle is also significantly less than that of the SI cycle. It is reported that overall thermal efficiencies of as much as 48% can be achieved by this process [10]. The HyS cycle is also environmentally friendly. The only products that are formed in the cycle, which are not recycled, are oxygen gas and hydrogen gas. The oxygen can be sold as a secondary product to facilitate the high cost of producing the electrolyzer.

One of the main problems with the HyS cycle is that sulphuric acid is formed during the electrolysis step. Concentrated sulphuric acid is a very weak acid and a poor electrolyte but in the diluted state it is a strong acid which will corrode most materials. The formation of sulphuric acid during electrolysis leads to material selection problems that need to be overcome to make the process economical and efficient.

The amount of research done and the corresponding literature on this cycle is extremely limited or remains unpublished. Reasons for the little amount of research on this subject can be attributed to the high capital cost involved in producing the electrolyzer and that development on this type of process only started in the 1970's, which makes it a relatively new technology.

1.1.3 Electrolyzer performance

The main indicator of an electrolyzer's performance is given by a polarization curve, which is the variation of the cells current density (A/cm^2) as a function of the applied voltage (V). Or simply stated, the curve is an indicator of the rate of chemical reactions taking place within the electrolyzer under the applied cell voltage [11]. Figure 5 is an illustration of a polarization curve for a SDE test unit constructed by Proton Energy Systems (PES). The figure clearly indicates the reduced cell voltage required for electrolysis if SO_2 is introduced into the process when compared to direct water electrolysis.

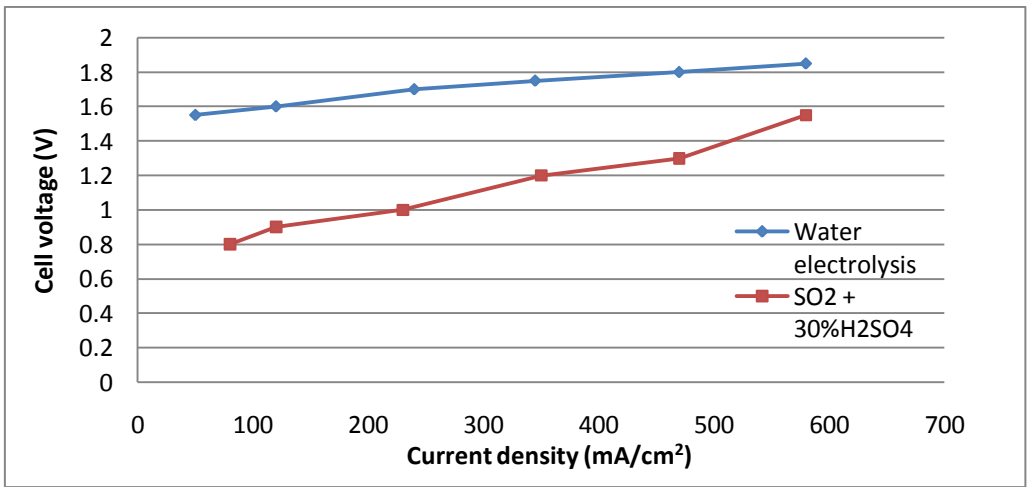

Figure 5: Polarization curves of the PES electrolyzer used for the electrolysis of water and the electrolysis of SO_2 dissolved in 30wt %H_2SO_4 modified after *J.L. Steimke et al.* (2005)

The Proton Energy Systems electrolyzer was a three cell stack assembly (Figure 6) with a reaction active area of 86cm^2 which could supposedly produce 20 litres of hydrogen gas per hour [12]. A commercially available 1kW *fuel cell* has a hydrogen gas consumption rate of ±840 litres per hour [13]. Clearly the production rates of hydrogen gas needs to be increased if it is to be used in combination with a fuel cell.

Figure 6: PEM electrolyzer stack assembly with 3 internal MEA's [8]

The issue of low production volumes can be overcome by increasing the cells' reaction active area. The conventional method to do this is by forming electrolyzer stack assemblies, as illustrated in Figure 6. Stack assemblies require a lot of equipment, such as multiple heat sources, inlets and outlets. The great deal of equipment and assembly detail makes it very difficult to produce an economically viable and efficient electrolyzer. Another possible solution is to linearly upscale the active cell area. This method will require less inlets and outlets and may facilitate a simpler manner to provide a uniform heat distribution for the reactions.

Apart from the results obtained for the Proton Energy Systems electrolyzer, the literature on upscaling of electrolyzers is very limited. However, a number of research reports on the upscaling of fuel cells are available, and since an electrolyzer is a fuel cell coupled in reverse[a], the findings of such upscaling are shortly reviewed.

Comparative studies of various sized fuel cells were conducted by L. Xianguo *et al.* (2006). They compared a 50cm^2 active area fuel cell to a linearly

[a] In an electrolyzer, electrical energy is used to produce the hydrogen gas whereas a fuel cell uses the hydrogen gas to produce electrical energy

upscaled 100cm^2 fuel cell. The polarization curves and power density curves, as constructed by L. Xianguo *et al.* (2006) are shown in Figure 7 and Figure 8, respectively.

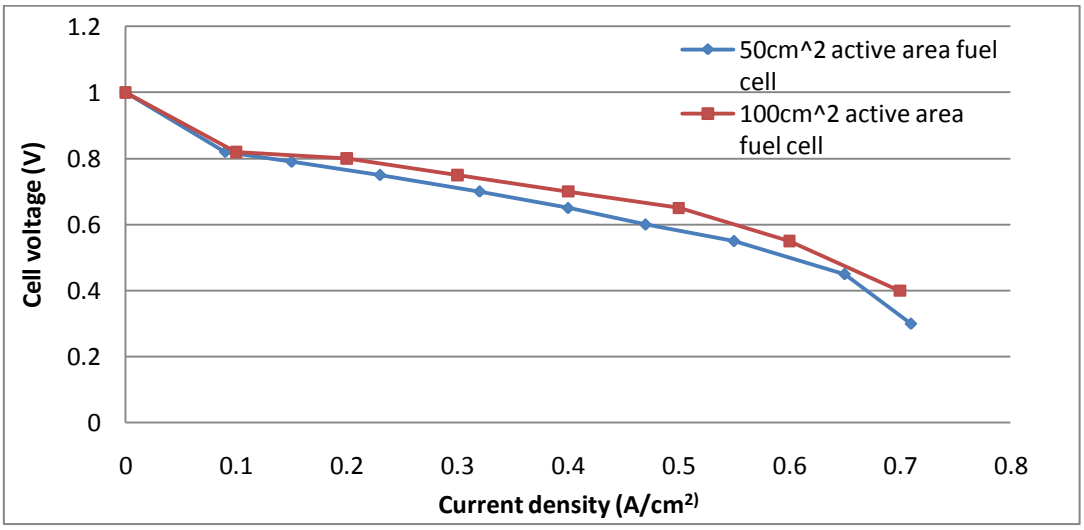

Figure 7: Polarization curves for a 50cm^2 and 100cm^2 active area fuel cell modified after L. Xianguo *et al*. (2006)

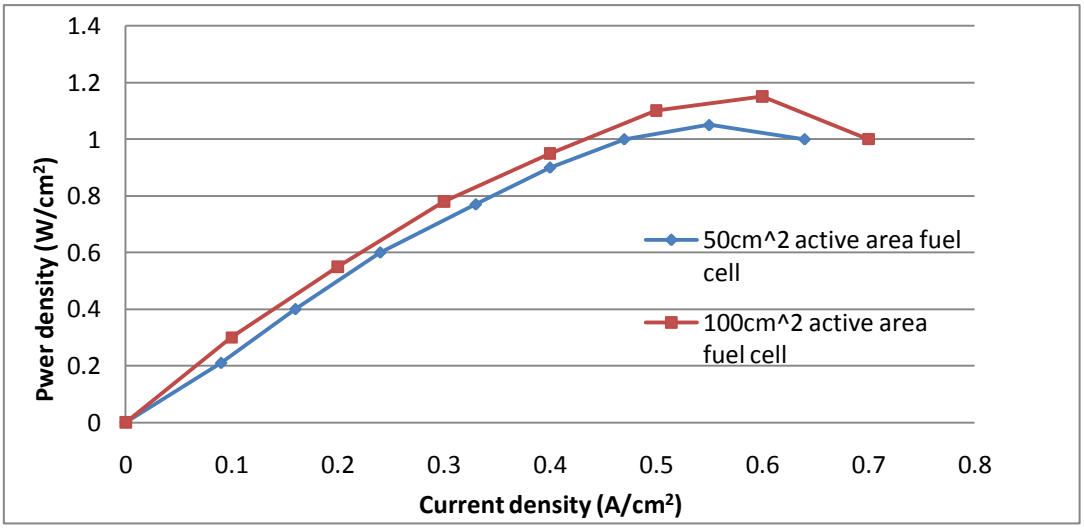

Figure 8: Power density vs. current density curves for a 50cm^2 and 100cm^2 active area fuel cell modified after L. Xianguo *et al*. (2006)

From Figure 7, it was noted that the V-I relations are very similar between the two different sized active areas, whilst Figure 8 shows that the 100cm^2 cell did have an increased power density of ±0.1W/cm^2. Thus it is likely that by linearly upscaling the active area of an *electrolyzer*, the production rates of hydrogen gas may be increased without a substantial increase in the applied cell voltage.

1.2 Problem Statement

The HyS cycle which makes use of a SDE, is a relatively new concept in the field of hydrogen production. This type of electrolyzer is a promising candidate for large scale hydrogen production because of the reduced cell voltage required for electrolysis.

Hydrogen fuel cells require large amounts of hydrogen gas in order to produce enough electrical energy for even the most basic of applications. Electrolyzers are normally formed into stack assemblies to increase the reactions active area, thereby increasing the hydrogen gas production rates. These stack assemblies require a lot of equipment, assembly detail and pose problems when it comes to providing adequate heat distribution for the process.

Based on the data obtained on the upscaling of fuel cells, it is thought that the hydrogen gas production rate can be increased by linearly upscaling the reactions active area. This method will have the advantage of less equipment, lower production costs, ease of assembly and better heat distribution for the same reaction active area.

1.3 Aim

The aim of this study is to design, construct and test an upscaled SDE test unit with emphasis on material selection and manufacturability to determine the effects of linearly upscaling the active area.

2 LITERATURE SURVEY

The literature survey covers the operation of a SDE as well as the components that form part of the SDE. Various parameters affecting the performance of electrolyzers are also addressed.

2.1 Background

The HyS cycle makes use of a SDE. As mentioned in the previous section, the main components of the SDE are the bipolar plates containing the flow fields and the MEA (Membrane Electrode Assembly). The MEA consists of two gas diffusion layers and two catalyst layers, one at the anode side and one at the cathode side. Figure 9 illustrates a simplified model of a SDE.

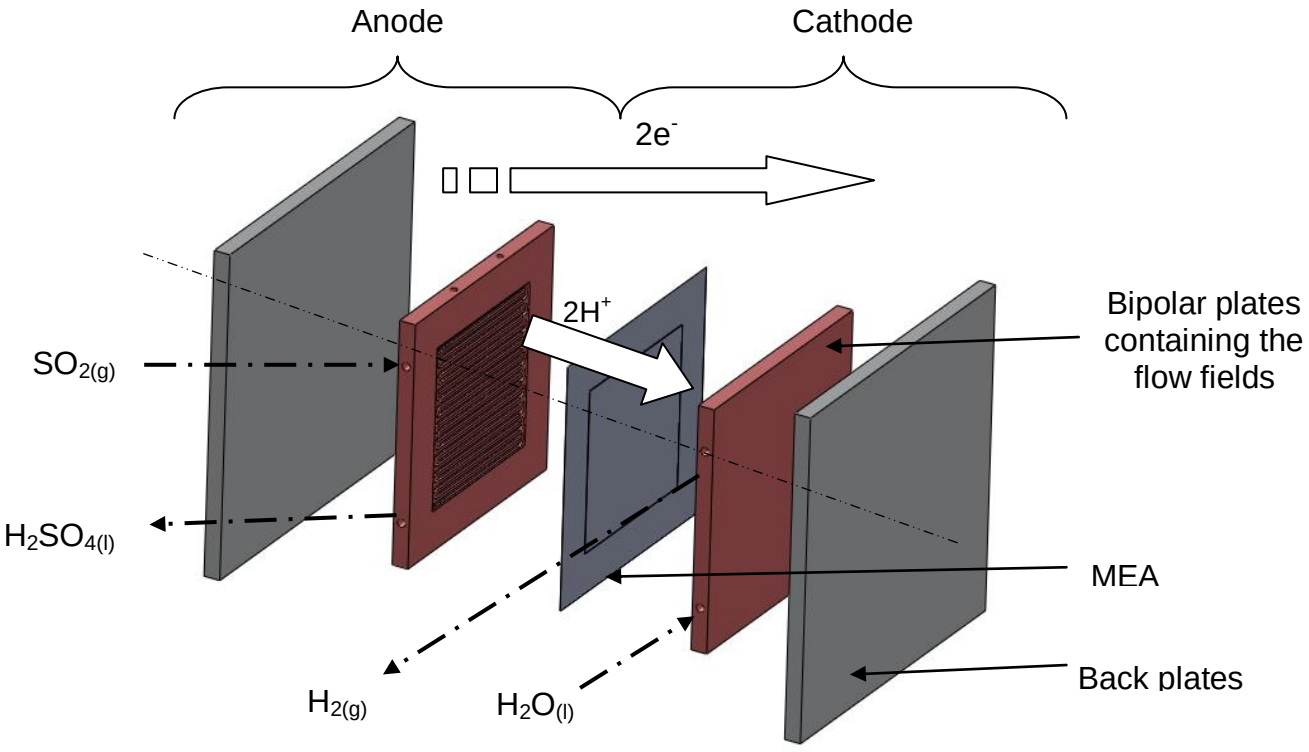

Figure 9: Simplified model of the SDE modified after D. Hobbs (2009)

The bipolar plates contain the flow channels necessary for the reactant delivery to the GDL's which usually contain the platinum catalyst for the reactions. SO_2 is fed to the anode side of the electrolyzer whilst deionised water is circulated through the cathode side, hydrating the membrane with the

necessary H_2O for the reaction. The SO_2 and H_2O are then oxidised by applying an electrode potential or current over the electrolyzer, thus forming hydrogen protons (H^+) and electrons (e^-). The electrons are then conducted to the cathode side by an external circuit whilst the protons are diffused through the proton conducting membrane, forming hydrogen gas at the cathode and sulphuric acid at the anode.

The chemical reactions taking place at the anode compartment are as follows [12]:

$$SO_2(g) + 2H_2O\ (aq) \rightarrow H_2SO_4\ (aq) + 2H^+ + 2e^-$$

Once the hydrogen protons and the electrons reach the cathode side, they are reduced to form hydrogen gas. The chemical reaction at the cathode is given by [12]:

$$2H^+\ 2e^- \rightarrow H_2(g)$$

2.2 Electrolyzer Components

2.2.1 Back plates

The main purposes of the back plates are to give the necessary support to the electrolyzer and provide a uniform pressure distribution over the cell to prevent leakage of the reactants/products from the flow channels. The two back plates are usually located at the axle ends of the electrolyzer. The electrolysis process requires elevated temperatures to be efficient which are supplied by heating elements that are commonly placed on the outer surface of the back plates. It would be advantageous to construct the back plates from a high thermally conductive material as to save on the operating costs of the heat source and increase the cells efficiency.

The literature shows that stainless steel (SS) is the more common back plate material. The PES cell made use of AISI 304 SS [14]. AISI 304 SS is part of the austenitic series of SS and has a very good corrosion resistance due to its high nickel and chromium content [15].

2.2.2 Current collectors

The purpose of the current collector is to serve as the base plate for the external circuit so that the circuit could effectively transport the electrons from the anode to the cathode. Copper alloys are typically used as current collectors due to their high electrical conductivity and relative low cost. If a stack assembly is to be created, it should be noted that an electrical insulation medium is to be inserted between the adjacent electrolyzers to prevent a short circuit.

2.2.3 Bipolar plates

Apart from the MEA, the bipolar plates are the most important components affecting the electrolyzer's performance, since it contains the flow fields for the reactant delivery and removal. A lot of research has been done on various configurations of flow fields and their influence on the efficiency of fuel cells. A lot less is known about the effect of the flow field configuration on the performance of an electrolyzer, the difference with respect to a fuel cell being that the flow field for the SDE will contain different products/reactants.

The type of flow pattern has an effect on the chemical reactions taking place within the flow field. Incorrect flow field design may lead to insufficient reactant and product removal causing decreased performance and ultimately decreasing hydrogen gas production rates. L. Xianguo *et al.* (2005) studied the effect of various flow field designs for fuel cells. There comparative study included a pin type channel arrangement (Figure 10), a parallel flow channel arrangement (Figure 11) and a serpentine flow channel arrangement (Figure 12).

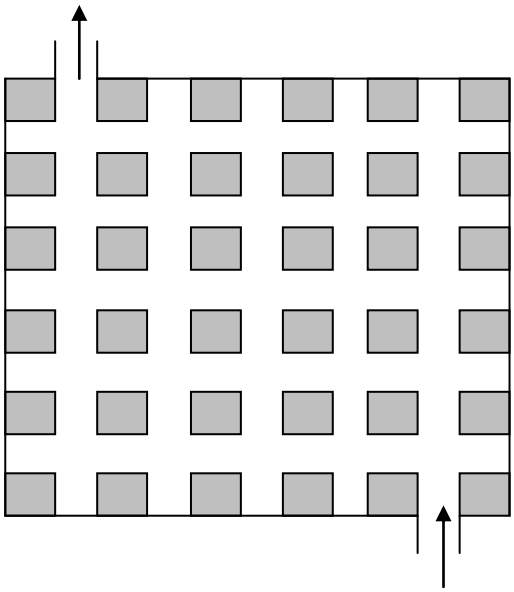

Figure 10: Pin type flow field design modified after L. Xianguo *et al.* (2005)

During their investigation they concluded that the pin type flow channel has the lowest pressure drop between the inlet and outlet. The low pressure drop is attributed to the fact that the fluid will take the path of least resistance, causing a non-uniform reactant distribution and stagnant areas being formed. These stagnant areas lead to valuable active area not being utilised.

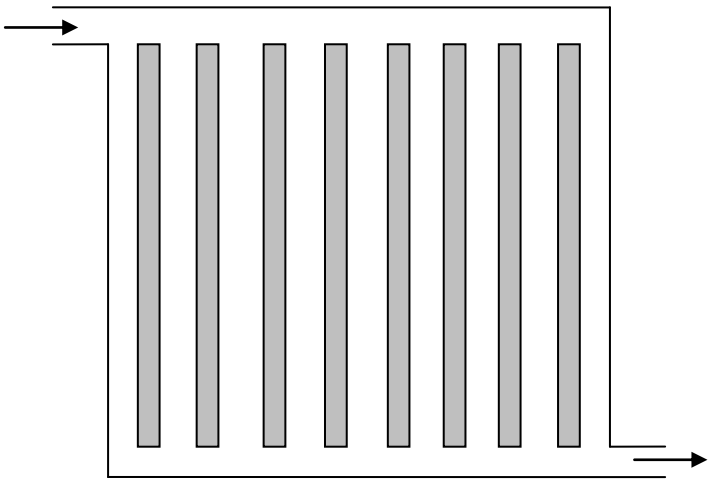

Figure 11: Parallel flow field design modified after L. Xianguo *et al.* (2005)

Furthermore, L. Xianguo *et al.* (2005) determined that the parallel flow field has a fairly uniform distribution of the reactants over the active cell area. However, the parallel channels are prone to the accumulation of gas bubbles. If gas bubbles are allowed to accumulate in a channel, the channel becomes unusable and the active cell area is reduced [16].

The parallel flow field is also prone to changes in flow rates which can easily cause a non-uniform flow distribution.

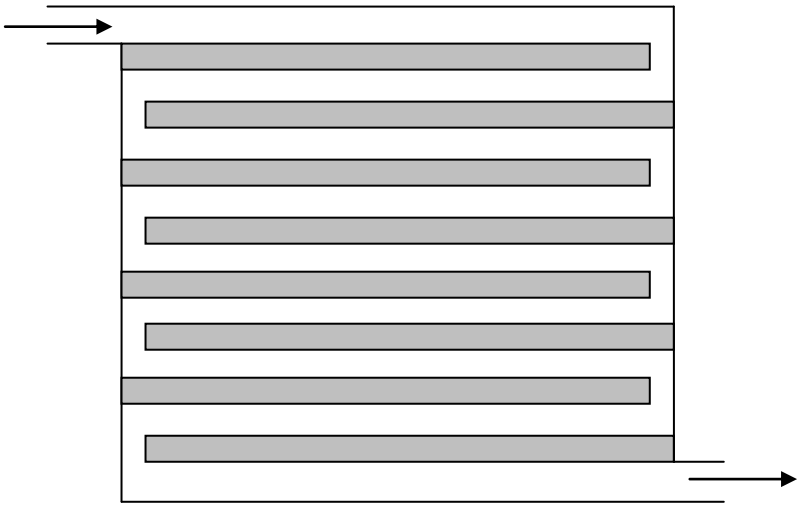

Figure 12: Serpentine flow field design modified after L. Xianguo *et al.* (2005)

L. Xianguo *et al.* (2005) concluded that the serpentine flow field achieves maximum usage of the active area. This design however suffers from high pressure drops which may cause regions of the membrane to become dehydrated but can be controlled by changing the geometry of the flow channels. If the pressure at the cathode is significantly lower than at the anode, it will enhance the chances of sulphur dioxide crossing the MEA and forming elemental sulphur at the cathode. The serpentine flow field is also prone to clogging but, despite this, it is the most favoured configuration currently under investigation.

A. Kumar *et al.* (2002) investigated the effect of channel dimensions and channel shapes on the flow distribution through the flow channel. They determined that the pressure drop can be reduced by using a rectangular cross section flow channel rather than a triangular or semi-circular cross section. Their results are summarized in Figure 13.

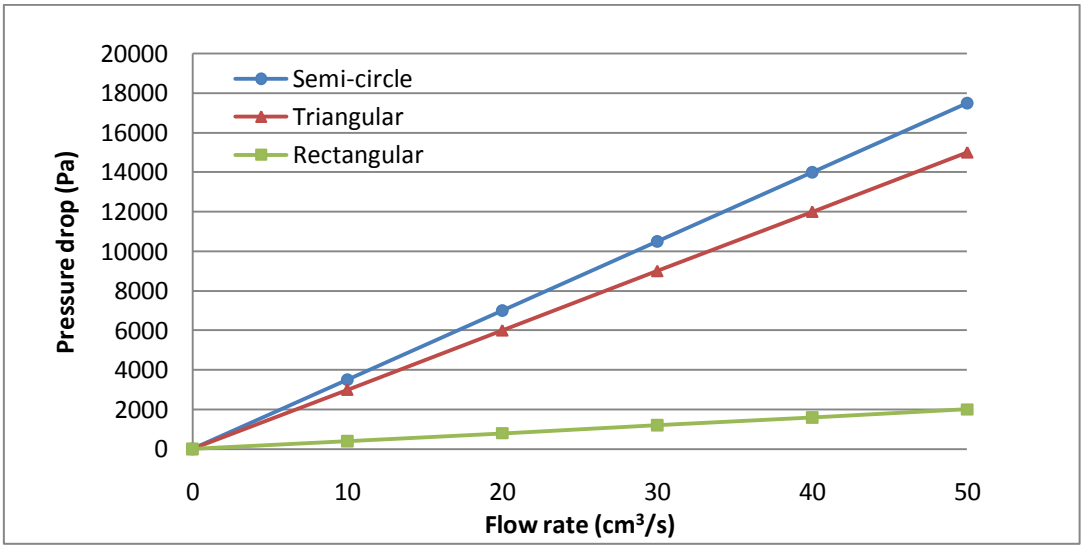

Figure 13: Calculated pressure drop indicating the advantage of using rectangular cross sections modified after A. Kumar *et al.* (2002)

These authors determined the optimum channel depth and width along with the land width for a 16cm^2 active area micro model PEM fuel cell. They concluded that by decreasing the land width, they increased the hydrogen consumption rate. It is thought that by decreasing the land width in the SDE, the SO_2 consumption rate will be increased, thus yielding a greater hydrogen production rate for the same amount of SO_2.

Bipolar plates are typically constructed from high electrically conductive materials with excellent corrosion resistance, the reason being that the bipolar plates need to conduct the electrons to the external circuit whilst resisting the effect of the produced sulphuric acid. The cell constructed by Proton Energy Systems used a Hastelloy series alloy whilst a cell constructed by The University of South Carolina (USC) used an unspecified grade of graphite [8]. The literature indicated that graphite was the most popular choice as an electrode material [15]. Graphite is a crystalline form of carbon consisting of basal planes of closely packed carbon atoms. The most important characteristic of graphite is its resistance to corrosion and it also has high electrical and thermal conductivity which makes it a promising candidate as an electrode material.

2.2.4 Gas diffusion layer and catalyst layer

The GDL is situated between the flow fields and the membrane. The GDL should ensure uniform transportation of reactants from the flow field to the membrane [17] and usually contains the catalyst [18]. The GDL is normally made out of a fibrous material such as PTFE (Polytetrafluoroethylene, Teflon) treated carbon paper or PTFE coated carbon cloth [19].

Palladium and platinum supported on carbon are currently favoured as catalytic materials for the electrolysis of sulphur dioxide. The type of catalyst influences the required cell voltage for the electrolysis and has a dramatic effect on the stable operation of the cell [20]. Various tests on the catalytic activity of palladium (Pd/C) and platinum (Pt/C) on carbon supports were conducted by D. Hobbs *et al.* (2009). It was concluded that the Pt/C catalyst showed higher catalytic activity at lower voltages than the Pd/C catalyst. The Pt/C catalyst also showed significantly less degradation than the Pd/C and is therefore favoured for use in the SDE.

Although carbon is favoured as the catalyst supporting medium it has the disadvantage of being oxidized to carbon dioxide at low voltages, leading to the degradation of GDL's. S. Maass *et al.* (2007) determined the effect of varying the applied voltage on the corrosion rate of carbon containing GDL's in PEM fuel cells. They concluded that the corrosion rate during the first 2 minutes of operation of the fuel cell was the highest after which it steadily declined with respect to the operation time. They also found that the cell voltage does have an impact on the corrosion rates, with severe corrosion rates occurring at cell voltages exceeding 1V (Figure 14).

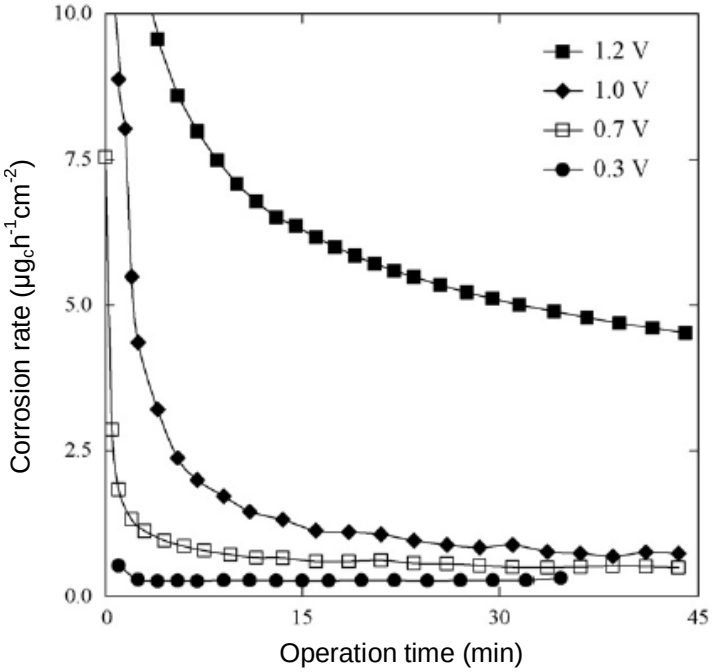

Figure 14: Corrosion rate of carbon electrodes used in PEM fuel cell at various cell voltages vs. fuel cell operation time [21]

2.2.5 Membrane

The function of the membrane is to facilitate the proton conductivity for the reactions, i.e. conduct the hydrogen protons from the anode side to the cathode, whilst blocking any other chemical species (including anions and electrons) [12]. If other chemical species, such as SO_2 are allowed to pass through the membrane, elemental sulphur can form and contaminate the MEA [14]. This contamination will lead to a decrease in reactions active area and ultimately a decrease in the hydrogen production volumes [22]. The more common membrane material currently favoured is Nafion. The Nafion polymer contains the chemical species (SO_3H) needed for proton conduction.

2.3 Electrolyzer Performance

In order for the electrolyzer to be as efficient as possible, it should have low operating cell voltages at high current densities. The theoretical cell voltage E, required by the electrolyzer is given by [14]:

$$E = E_{rev} + \eta_a + \eta_c + \eta_{ohm} + \eta_{hw}$$

with E_{rev} - Reversible cell potential
η_a - Anode overpotential
η_c - Cathode overpotential
η_{ohm} - Ohmic losses
η_{hw} - Hardware losses

Overpotential is defined as the difference between a half reaction's thermodynamically determined reduction potential and the actual potential at which the redox reaction takes place [23]. The value of the overpotential is a function of the catalyst surface area and type as well as the acid concentrations. The electrolyzer will also experience an increased cell voltage due to Ohmic losses within the cell, these Ohmic losses are due to the electrical resistance of the reactants within the cell. The cell voltage required for electrolysis is also dependant on the hardware losses of the cell. Hardware losses arise from the electrical resistance of the materials used to construct the cell.

From the above equation it is evident that larger sized reaction active areas will require a greater cell voltage for the electrolysis process. J.L. Steimke *et al.* (2006) stated that the Ohmic losses can be reduced by decreasing the distance between the electrodes. Furthermore, they concluded that an increase in the SO_2 concentration at the anode side will decrease the anode overpotential. Hardware losses can be reduced by precise material selection and hardware design.

2.4 Purpose of Study

It is thought that the hydrogen production rates of the SDE can be increased by linearly upscaling the reaction's surface area. Thus, the purpose of the study is to design, construct and test an upscaled SDE as to determine the effects of linear upscaling. The following design considerations were incorporated in the design of the SDE:

- Material selection
    - Materials are required to withstand temperatures of up to 200°C.
    - Materials must be able to withstand corrosion by sulphur dioxide and sulphuric acid, where applicable.
    - Materials with high thermal and electrically conductivities should be used to limit hardware losses and reduce operational costs.
- Bipolar plate design
    - As much as possible of the reaction active area should be utilised.
    - Design must prevent accumulation of gas bubbles.
    - The design must facilitate a much larger MEA than conventional test unit cells.
    - Bipolar plates must be able to withstand an internal pressure of at least 100kPa.
    - Bipolar plates must have room to measure the applied cell voltage and room for a thermocouple.
- Heating pad design
    - The heating element must be able to heat the flow fields to 80°C.
    - The heating element must cover the entire area of the bipolar plate.
    - The element must contain a female kettle plug to conform to a current test bench.

- Peripherals
    - The cell should be easily assembled and disassembled.
    - The cell should be air tight.
    - The back plates must provide an even pressure distribution over the cell.
    - The cost in producing the SDE should be as low as possible whilst taking performance into account.
- Test requirements
    - Compare the results from the upscaled cell to a commercially acquired cell with a smaller active area under the same testing conditions[b]. For this comparative study, testing needs to be done at 80°C with the same MEA's and reactant flow rates.
    - Compare the results of the upscaled cell to the results found in the literature.
    - Conduct tests in an accurate and safe manner.

2.5 Summary

The literature survey addressed the operation of a SDE and its main components. The function of each component was discussed along with the common material used to construct the component. J.L. Steimke *et al.* (2006) proposed various methods that can reduce the cell voltage which were considered in the design.

[b] Commercially available SDE with an active area of 25cm^2 acquired from Giner Electrochemical Systems (GES).

3 ELECTROLYZER DESIGN

In order to determine the effects of linearly upscaling a SDE, a test unit was designed based on the design considerations as well as designs set forth in the literature. The SDE model is indicated in Figure 15 and is comprised of the following components:

- Heating pad
- Back plates
- Electrical insulation
- Current collectors
- Bipolar plates containing the flow fields
- MEA
    - Membrane
    - Gas diffusion layers
    - Catalyst layers

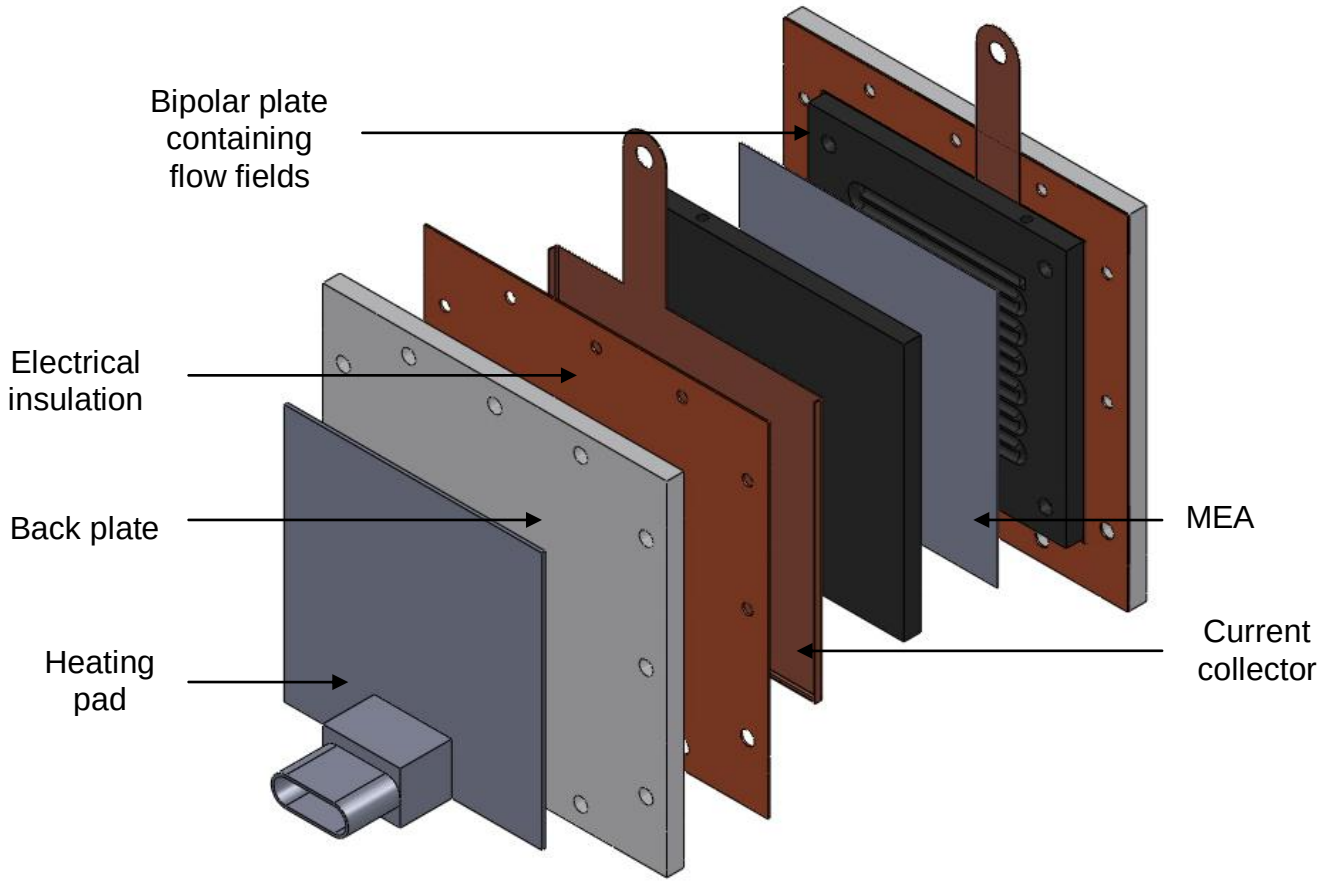

Figure 15: Exploded view of the model of the electrolyzer concept design

3.1 Membrane Electrode Assembly

A smaller commercially available cell acquired for comparative purposes has an active area of 25cm^2, thus it was necessary to locate two identical MEA's, one with an active area of 25cm^2 and one with a sufficiently larger active area in order to study the effects of upscaling. Commercially available MEA's have typical active areas of 25cm^2, 50cm^2 and 100cm^2. A 100cm^2 MEA was chosen because of its significantly larger active area as compared to the commercially acquired cell. The chosen MEA is known as a 5-layer MEA consisting of two GDL's containing two Pt/C catalyst layers with a loading of 0.5mg/cm^2 and the Nafion 117 which was deemed appropriate from previous experience for SO_2 electrolysis.

3.2 Material Selection

The material selection process was carried out by using Computer Aided Design (CAD) software such as the Cambridge Engineering Selector (CES) along with a technique as described by M.F. Ashby (2005). CES is a material database which was used to identify suitable materials for each component.

The material selection process was carried out by first determining the function of the component and applying limiting values on the material properties needed so that the component can perform its intended function. If sufficiently few materials remained after the limiting values on the material properties were applied, the literature was consulted to determine the best suited candidate material. However, if limiting values on the material properties returned a great number of possible candidates, a material index was derived to rank the possible candidates after which the literature was consulted to identify the best suited material. The steps performed in the selection process are illustrated in Figure 16 [24] and further details on the derivation of material indices are presented in Appendix A.

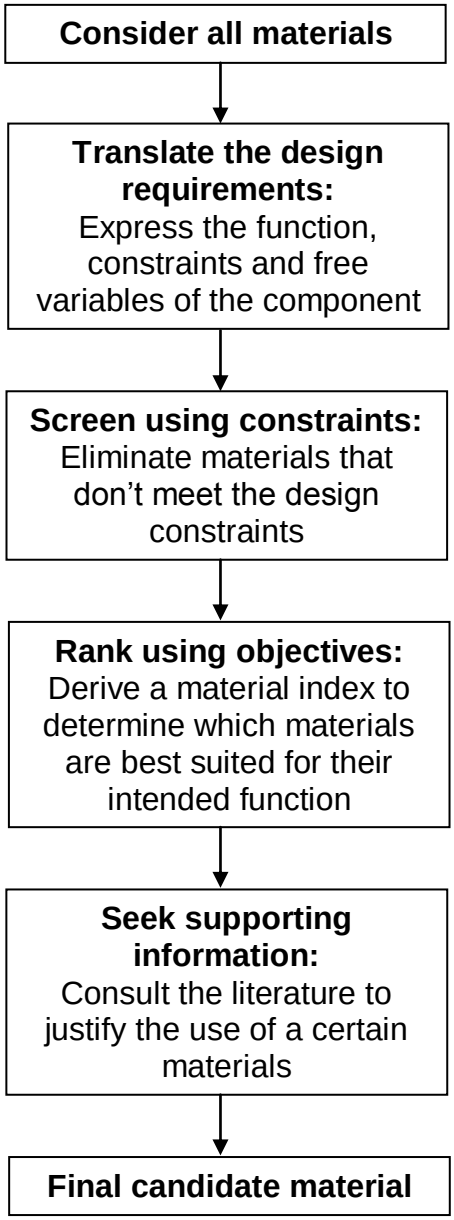

Figure 16: Material selection procedure modified after M.F. Ashby (2005)

3.2.1 Back plates

Candidate materials for use as back plates were identified by applying limits on the maximum operating temperature and maximum shear stress. The remaining candidates were then ranked by maximizing the materials thermal conductivity whilst minimizing the material density. The material index used for finding the best suited candidates was derived as $M_1=\lambda/\rho$,

where λ - Thermal conductivity of the material (W/mK)

ρ - Density of the material (kg/m^3)

The back plates will not be in contact with any acids, but using a material with very good corrosion resistance will be advantageous in case of accidental spillage. Materials that conformed to the requirements was found to be the following candidates:

Table 1: Back plate materials

Wrought aluminium alloy, 5005 (H4, H6 and O)[c]
Wrought aluminium pure, 1050A (H9 and O)
Wrought aluminium pure, 1080 (HB and O)
Wrought aluminium pure, 1200 (H5, H9 and O)

UNS 5005 aluminium alloy exhibit higher thermal conductivities and have better corrosion resistance than the other possible candidates [15] and was accordingly selected as the back plate material.

3.2.2 Electrical insulation

The properties of the polymer family of materials were screened to find possible materials for use as an electrical insulation medium. Since electrical insulation mediums generally exhibit electrical resistivities in excess of $1e^6\Omega m$, it was used as a limiting value on the material property. The maximum operating temperature was subjectively chosen as 200ºC and was also applied as a limiting value. The appropriate candidates were then narrowed down by maximizing the thermal conductivity of the materials. The following candidates were identified for use as an electrical insulation medium:

Table 2: Electrical insulation materials

Silicone Elastomer (Eccosil)
Epoxy (Novolak)
Phenol Formaldehyde (Bakelite)

Upon further revision of the possible candidates, Eccosil (silicone elastomer) was chosen as the best possible material since it has the added advantage of

[c] *H* and *O* refer to different types of heat treatment techniques used in producing the alloy.

its elasticity characteristics that would protect the other components of the electrolyzer from failure due to impact. The silicone elastomer is also easily obtainable, inexpensive and available in a great number sheet sizes and thicknesses.

3.2.3 Current collector

An appropriate current collector material was found by applying a limiting value on the maximum operating temperature of the materials, this temperature was subjectively chosen as 150ºC. The remaining candidates were then screened by adjusting the electrical resistivity of the materials along with the material price until only a few candidates remained. All the possible candidates fall under the high copper content family (Table 3).

Table 3: Current collector materials

Electrolytic tough pitch copper (UNS C1xxxx)
High conductivity copper (UNS C18xxx, UNS C15xxx)
Phosphorous de-oxidised copper (UNS C12xxx)

UNS C12220 copper alloy was selected as the current collector material since it has nearly as high electrical conductivities than the other candidates but has the added of advantage of being easily obtained locally at a fraction of the price of the other candidates.

3.2.4 Bipolar plate

Material properties under consideration in the selection process for a bipolar plate material included very good resistance to strong acids as well as a maximum operating temperature of 150ºC. A material index was derived to determine which of the possible candidate materials will best serve as a bipolar plate material. The material index took the thermal conductivity, material cost and density into account.

The index was derived as $M_2=\lambda/C_m\rho$,

where λ - Thermal conductivity of the material (W/mK)

C_m - Material cost per kg. (ZAR/kg)

The possible candidates for use as bipolar plates are listed in Table 4.

Table 4: Candidate materials for use as bipolar plates

Carbon (Recrystallised)
Concrete (High alumina cement and sulphate cement)
Graphite (Electrographite)
Al-20SiC (Duralcan)

From the data obtained in the literature, it was expected to find graphite in the list of possible materials, however, Duralcan has supposedly better corrosion resistance. The literature was consulted on the chemical resistance of Duralcan in a sulphuric acid environment, and virtually no reliable sources could be found. It is also extremely difficult to locate with only a few American companies producing it for aeronautical applications.

It was decided to use as close to zero porosity graphite as possible since it has been tried and tested and showed favourable results. Upon further inspection into concrete as a candidate material, it was noted that it has an extremely high electrical resistivity and was therefore discarded.

3.3 Bipolar Plate Design

The design requirements state that us much as possible of the active area has to be utilised which can be achieved by using the serpentine flow channel configuration. The only concern in using this configuration is the increased pressure drop which may lead to regions of the membrane to become dehydrated and the increased possibility of SO_2 diffusing through the MEA.

The increased pressure drop will be counteracted by using a rectangular flow channel cross section, rather than a triangular or semi-circular cross section. In this design, use is made of 180° U-bends rather than two 90° elbows currently employed in the flow path of fuel cells reviewed. It is thought that the use of U-bends will decrease the pressure drop through the flow channels.

The pressure drop through a flow channel is given by:

$$\Delta P = h_m + h_l$$

$$h_m = f\frac{l}{D}\frac{V^2}{2g}$$

$$h_l = K_l\frac{V^2}{2g}$$

with

	ΔP	-	Pressure drop (kPa)
	h_m	-	Mayor losses term (kPa)
	h_l	-	Minor losses term (kPa)
	K_l	-	Minor loss coefficient
	l	-	Channel length (m)
	f	-	Friction factor of material
	V	-	Fluid velocity (m/s)
	g	-	Gravitational constant (m/s^2)
	D	-	Hydraulic diameter of flow channel (m)

As a first approximation on the impact of using U-bends, the pressure drop through a flow channel at various mass flow rates was calculated using the Engineering Equation Solver (EES) with the following assumptions:

- Water was used as the fluid with a density of $1000kg/m^3$ and dynamic viscosity of $1.12e^{-3}N.s/m^2$.
- The K_l factor for 90° elbows are 0.3 and 0.2 for U-bends [25].

The results obtained for the pressure drop through the flow channel are illustrated in Figure 17 with the details of the calculations presented in Appendix B.

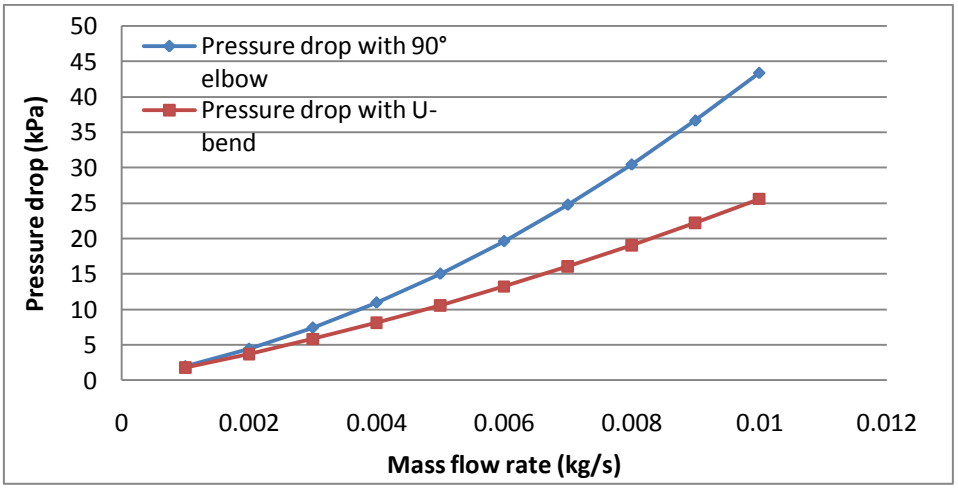

Figure 17: Calculated pressure drop through rectangular flow channels as a function of the mass flow rate

It was found that the pressure drop was not substantially reduced at the expected low flow rates of the SDE (0.002-0.003kg/s) when U-bends were employed.

To further evaluate the linear pressure distribution through the flow channels for the case of the two 90º elbows as well as the case of U-bends, a Computational Fluid Dynamics (CFD) analysis was performed using ANSYS. The results of the pressure distribution through the anode and cathode are presented in Figure 18 and Figure 19, respectively.

The pressure distributions on the anode and cathode sides were simulated with the following assumptions:

- Sulphur dioxide gas with a flow rate of 500ml/min will be delivered to the anode (expected testing flow rate determined from previous experience).
- Water flow rate of 150ml/min will be delivered to the cathode (expected testing flow rate determined from previous experience).
- Atmospheric temperatures.

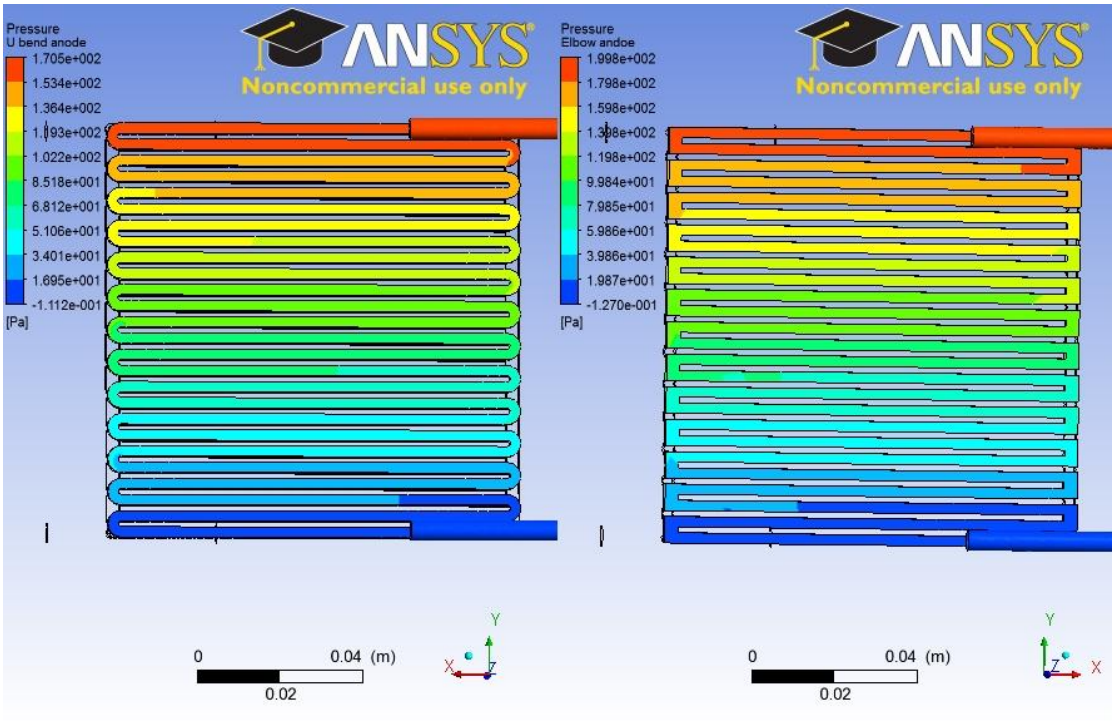

Figure 18: Pressure distribution at the anode using U-bends (left) and 90° elbows (right) with a sulphur dioxide gas flow rate of 500ml/min

The ANSYS simulations showed that by employing U-bends, the pressure drop between the inlet and the outlet was reduced from 0.2kPa to 0.17kPa. The use of U-bends also resulted in a lower negative pressure at the anode outlet.

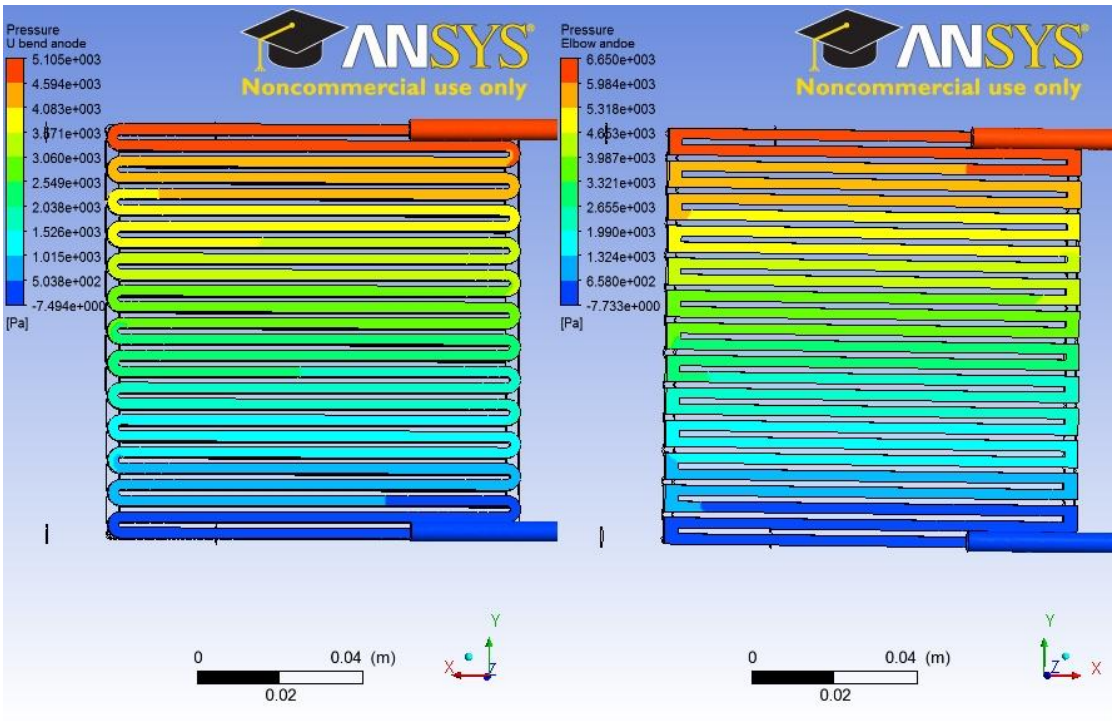

Figure 19: Pressure distribution at the cathode using U-bends (left) and 90° elbows (right) with a water flow rate of 150ml/min

The pressure drop at the cathode when U-bends where employed was determined as 5.12kPa whilst using 90° elbows resulted in a pressure drop of 6.65kPa. The use of U-bends at the cathode also resulted in a lower negative pressure at the cathode outlet.

It was concluded that the use of U-bends will reduce the possibility of SO_2 crossover from the anode to the cathode by reducing the negative pressures located at the anode and cathode outlets. U-bends also have the advantage of being easily machined and is the therefore favoured configuration.

The flow channel geometry was chosen as to utilize the maximum amount of surface area, decrease the Ohmic losses and require only basic machining techniques and is presented in Figure 20.

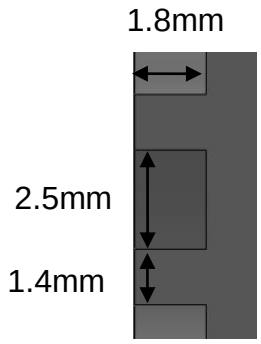

Figure 20: Channel geometry indicating the channel depth, width, land width and adjacent channels

To prevent the accumulation of gas bubbles in the flow channels, port holes were used to connect the inlet and outlets to the flow channel. The functions of the port holes were to reduce the size of gas bubbles travelling through the flow channels thereby decreasing the probability of clogging and also ease the machining of the component.

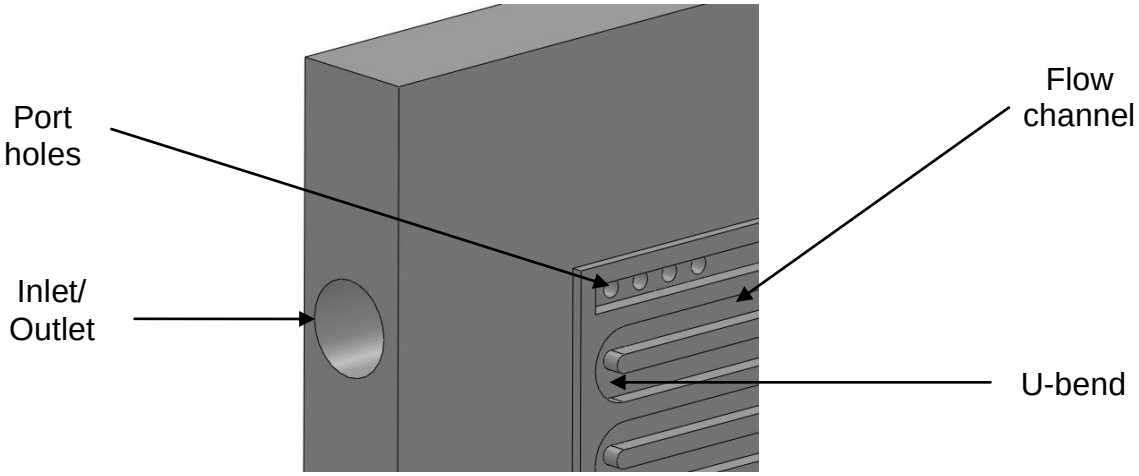

Figure 21: Bipolar plate indicating port holes and U-bends

Channels to the side of the bipolar plate are provided to facilitate room for a thermocouple so that the temperature distribution may be identified. In order to control the operating temperature of the electrolysis process, the thermocouple is connected to a relay. In order to measure the required testing temperature as close as possible to the operating temperature, the thermocouple channels were as close to the flow channel as possible. The distance between the thermocouple channel and the flow channel was 2.2mm. Decreasing the distance may result in failure of the part during manufacturing due to brittle nature of graphite.

Room for banana plugs are provided to measure the cell voltage over the bipolar plates. The common practice in fuel cell and electrolyzer testing is to measure the cell voltage across the bipolar plates rather than the current collector. The provided thermocouple channels and room for the banana plugs are indicated in Figure 22.

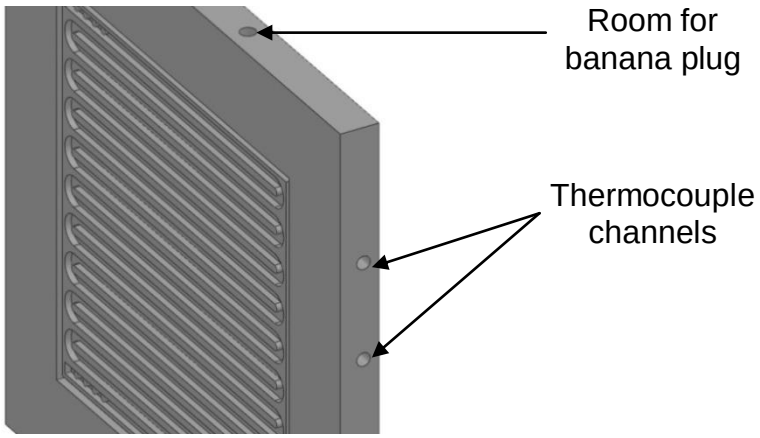

Figure 22: Bipolar plate indicating thermocouple channel and banana plug hole

An increased pressure can also be used to improve the reaction kinetics within the electrolyzer, current high pressure test units under development have been tested up to an internal pressure of 2MPa. Although the testing requirements only stipulate an internal pressure of 100kPa, a structural finite elemental analysis was performed with an internal pressure of 2MPa applied to the internal geometry of the bipolar plate. The structural analysis was performed using ANSYS and further details of the simulation are addressed in Appendix B.

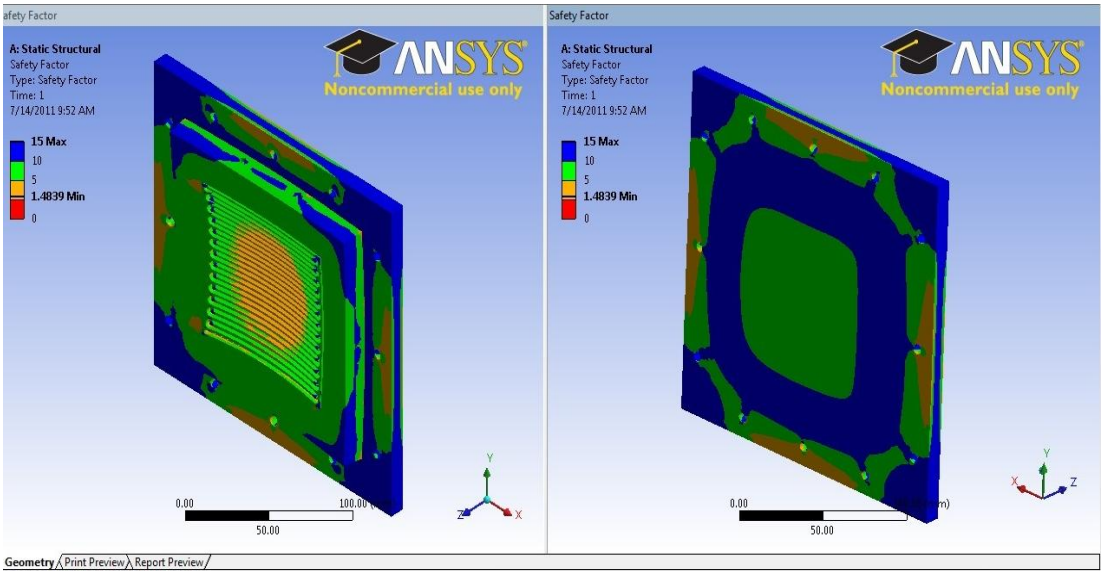

Figure 23: Safety factor distribution with a 2MPa internal pressure applied to the internal geometry

The minimum safety factor was determined as 1.48 and was located at the port holes joining the inlet and outlets to the flow channels. The safety factor distribution is illustrated in Figure 23. It was concluded that the cell will easily resist the specified 100kPa internal pressure. ANSYS was used to determine the maximum internal pressure that the cell could withstand. The maximum internal pressure was calculated as 3MPa, increasing the pressure will not cause catastrophic failure of the cell but the sections between the port holes will fail. This may cause too large bubbles to form and will decrease the efficiency of the cell.

3.4 Heating Pad Design

The electrolyzer requires elevated temperatures ranging from 80°-100°C to improve the reaction kinetics. The elevated temperature is supplied by a heating element located on the back plate of the cell. The power required by the heating pad was calculated using the fundamentals of heat transfer:

$$q = \frac{\Delta T}{\sum R_t}$$

where
- q - Power required by heating pad (W)
- ΔT - Temperature difference that q has to facilitate (K)
- ΣR_t - Sum of the thermal resistances of the materials due to conduction through the electrolyzer and convection at the heat pad (K/W).

Calculations were carried out using EES based on the following assumptions:

- Outer edges are adiabatic.
- Convection was only considered on the heat pad side and radiation was neglected due to expected relative low impact.
- Steady state conditions assumed.
- Thermal insulation (Thermal ceramic, Type AL-45) is placed on the outer edges of the heating pad.

It was determined that a 60W heating pad will be required to get the flow fields to a temperature of 100°C with the details presented in Appendix C. Ohm's law was used to determine the type of material for use as an electrical resistive wire required to construct the heating pad. Ohm's law states that:

$$V = IR$$

and

$$P = VI$$

where
- P - Power required by heating pad (60W)
- V - Applied voltage (230V provided by the test bench)
- I - Current induced by the applied voltage (A)
- R - Electrical resistance of the wire (Ω)

From this it was calculated that a 0.07mm NiChrome 80 cold drawn wire with a corrected length of 3.14m will be ideal to construct the heating pad. The design calculations are presented in Appendix C.

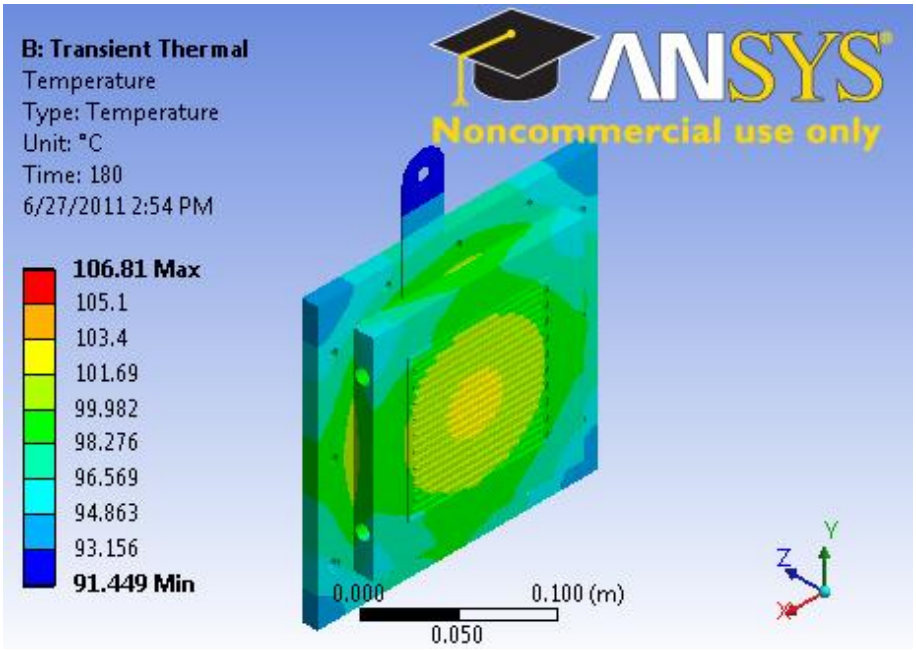

Figure 24: Transient heat distribution through cell with 750W heat flow after 3min

The heating pad calculations were done with the assumption that the process is a steady state process, thus requiring a great deal of time for the bipolar plates to reach the correct operating temperature. It was decided to purchase a 750W heating pad to save on construction and testing times. In order to protect the membrane from excessive temperatures caused by the overpowered heating pad, a relay is used for the temperature control. A finite elemental analysis was performed using ANSYS to identify the transient heat distribution through the cell based on a 750W heating pad (Figure 24). The finite element analysis indicated that the 750W heating pad only requires 3min to get the flow fields to a temperature of ±100°C whilst the 60W heating pad requires roughly one hour.

3.5 Peripherals

The back plates is to be provided with room for 12xM6 ISO threaded holes to ensure an even pressure distribution over the cell. To ease the assembly and disassembly of the cell, the electrical insulation and current collector is to be glued to the back plates by applying a thin layer of RTV (Room Temperature Vulcanizing) silicone adhesive to the components.

In order to easily remove and insert the electrolyzer into the test bench, a bracket was designed. A leakage tray was also designed to protect the test bench from accidental acid leakage. The bracket and tray is to be made from carbon steel and Perspex, respectively.

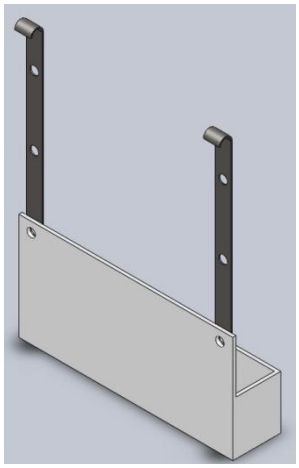

Figure 25: Bracket and leakage tray sub-assembly

To prevent leakage in the SDE, a recess was incorporated into the bipolar plates. The recess functions are to centre and contain the GDL so that the membrane may serve as the gasket between the two bipolar plates. Two M3 ISO threaded holes is provided for the inlet and outlet components. A finite element structural analysis was performed using ANSYS to determine the deflection of the plates with a 2MPa internal pressure applied to the cell. The results of the deformation distribution (Figure 26) indicated that the maximum deflection occurred at the centre of the bipolar plates and was determined as 0.13mm. It was concluded that under the stipulated testing pressure of 100kPa, the cell will not be deformed significantly enough to cause leakage.

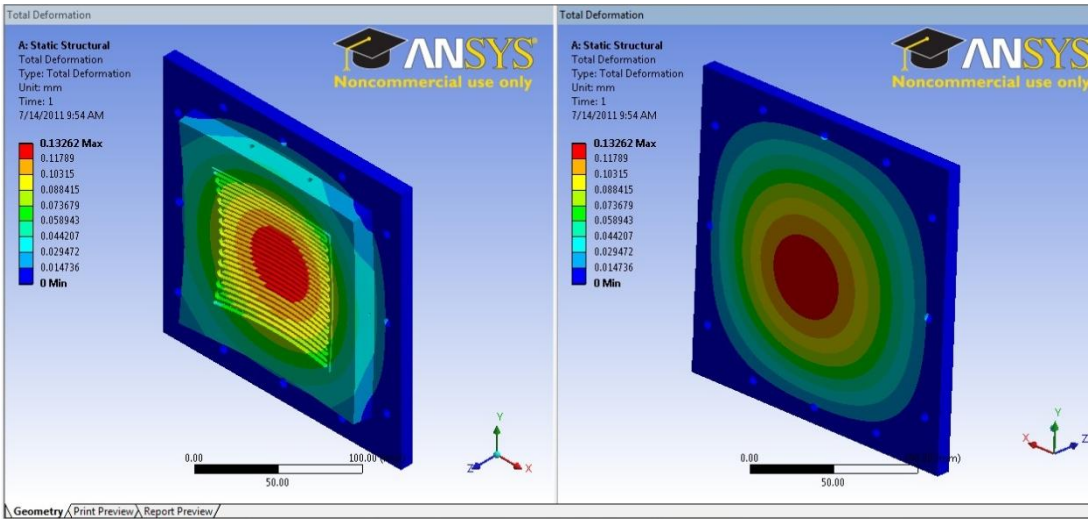

Figure 26: Deformation distribution with a 20 bar internal pressure applied to the internal geometry of the bipolar plates

To ensure safe operation and testing of the cell, the Material Safety Data Sheets (MSDS) were obtained for the reactants and products involved. Details of the safety aspects are discussed in Appendix D.

4 MANUFACTURING AND ASSEMBLY

The manufacturing and assembly of the SDE is discussed next. Unless otherwise stated, the materials were procured and manufactured at a workshop located at The School of Mechanical Engineering at the North-West University with the design drawings presented in APPENDIX G. The assembled electrolyzer is presented in Figure 27.

Figure 27: Final assembly of the sulphur dioxide depolarized electrolyzer

4.1 Back Plates

The 200x200x10mm back plates are indicated in Figure 28 and were machined according to drawing SDEBP1.

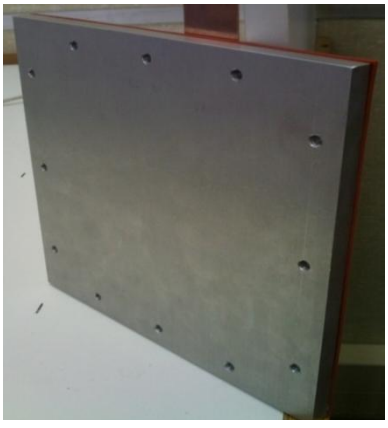

Figure 28: UNS 5005 aluminium back plate

4.2 Current Collector and Insulation

The UNS C12220 copper alloy was supplied by Copalcor (Pty) Ltd and machined according to drawing SDECC1. The Eccosil was cut from a standard sheet according to drawing SDEEI1. The initial design required that the silicone sheet covers the entire back plate, the sheet was later cut to a smaller dimension to ease assembly between the bolts that are inserted through the back plates.

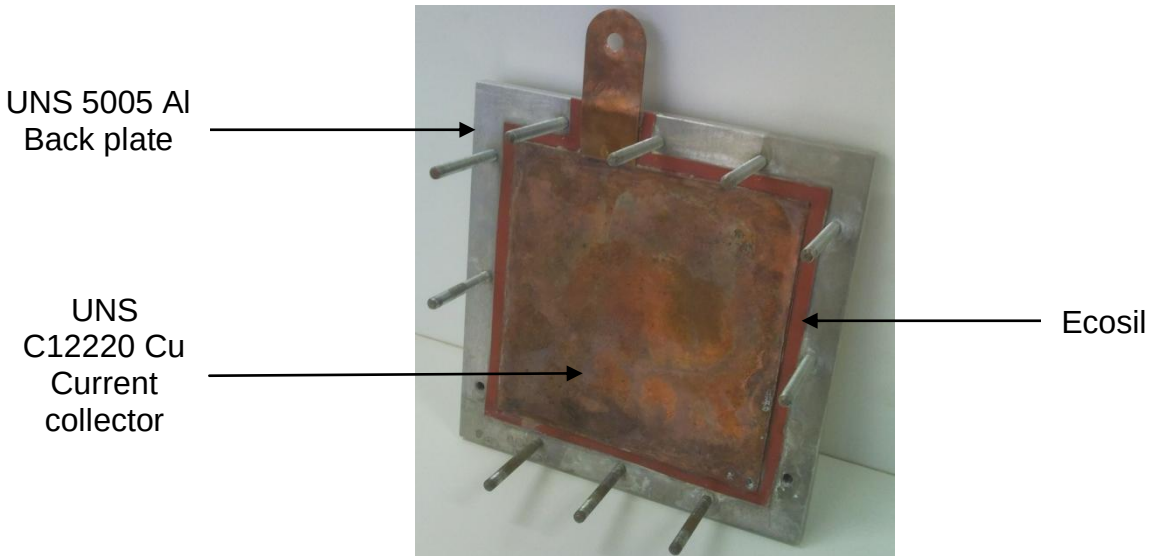

Figure 29: Electrolyzer sub-assembly consisting of a back plate, current collector and electrical insulation

4.3 Bipolar Plates and Inlet/Outlet Components

The bipolar plates were manufactured from ATJ isomolded graphite supplied by GrafTech (Pty) Ltd and machined using a CNC (Computer Numerically Controlled) machine according to drawings SDEFF1 and SDEFF2. The ATJ isomolded graphite was the lowest porosity graphite that could be locally obtained. The bipolar plates contained a 0.35mm recess for the GDL's, the flow channels for the reactants, channels to measure the temperature distribution, room for the banana plugs and the M3 ISO threaded inlet and outlet holes.

Figure 30: ATJ isomolded graphite bipolar plate containing the PTFE inlet and outlet components

The inlet and outlet components were manufactured from PTFE according to drawing SDEIO1 using a lathe. The reason for choosing PTFE is that it is one of the few materials that can resist the strong acid environment and has the required elasticity as to provide an adequate seal. The components needed to be custom made since no such fittings could be obtained.

Figure 31: M3 ISO threaded inlet and outlet components manufactured from PTFE

4.4 Heating Element

The heating element (Figure 32) is known as a flat clad element heater and was purchased from Hi-Tech Elements (Pty) Ltd. The element has a heating area of 150x150mm, the same area as the bipolar plates, and had a maximum power output of 750W with a kettle plug attachment. The heating element was secured to the back plate by using thin back strips of copper sheet along with the M6 ISO threaded holes in the back plates.

Figure 32: Flat clad element heater acquired from Hi-Tech Elements (Pty) Ltd.

4.5 Bracket and Leakage Tray

The Perspex used for the leakage tray was cut according to drawing number SDELT1 using a laser cutter and assembled whilst the carbon steel only required 6x7mm holes to be drilled. The assembly was secured to the back plate by using the same bolts that secure the entire electrolyzer.

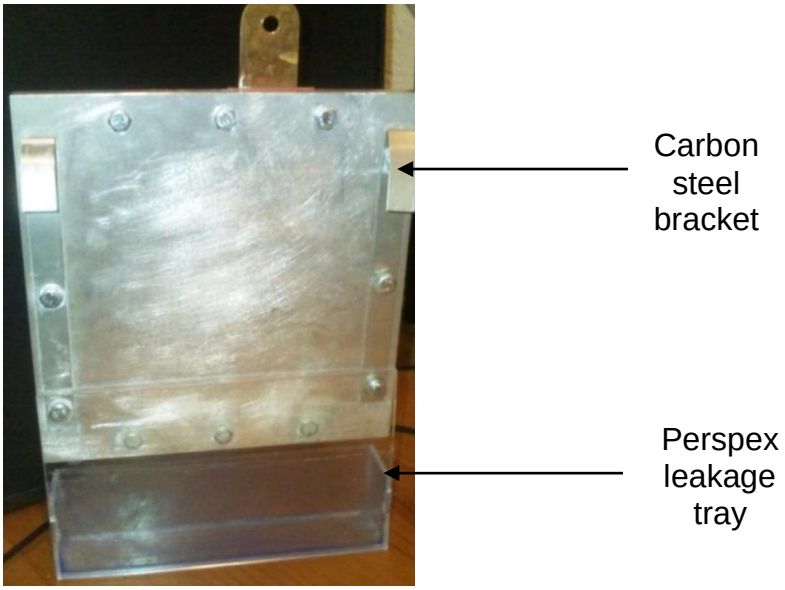

Figure 33: Bracket and leakage tray assembly

4.6 Electrolyzer Assembly

The following assembly procedure was followed to ensure the correct operation of the cell:

1. The bipolar plates were aligned in the centre of the back plate sub-assembly (with the bolts already in position).

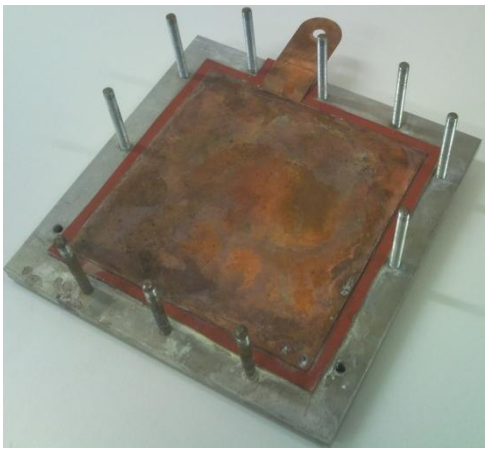

Figure 34: Bipolar plates aligned in the centre of the current collector (Step 1)

2. The MEA was placed on the bipolar plates so that the GDL is positioned over the recess machined into the plates.
3. The other bipolar plate was placed over the exposed GDL ensuring that both plates were exactly aligned. Great care was taken to ensure that the MEA doesn't shift during this step.

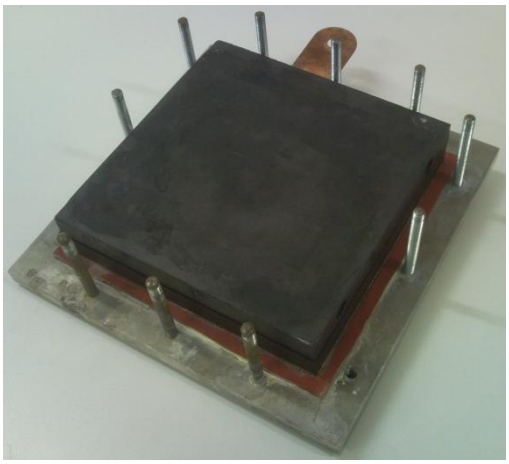

Figure 35: Electrolyzer assembly with both bipolar plates in position (Step 3)

4. The remaining back plate sub-assembly was then placed over the bipolar plate and the bolts tightened with a torque wrench.

5 EXPERIMENTAL SET-UP AND TEST PROCEDURE

The purpose of the project was to determine the effects of linearly upscaling a SDE. To study the effects of upscaling, the following variables had to be measured:

- Current
- Cell voltage
- Resulting hydrogen gas production rate

The current and cell voltage values were measured using the power supply which was coupled to current collector and banana plugs whilst the hydrogen gas production rates were measured using a bubble flow meter. The bubble flow meter is a simple yet highly accurate apparatus used for measuring flow rates [26]. It involves timing the movement of bubbles of a soap film caused by the produced hydrogen gas up a tube of known volume.

5.1 Test Bench Set-Up and Operation

A test bench was constructed at the NWU's School of Chemistry. A schematic and photo of the test bench lay-out is illustrated in Figure 36 and Figure 37, respectively.

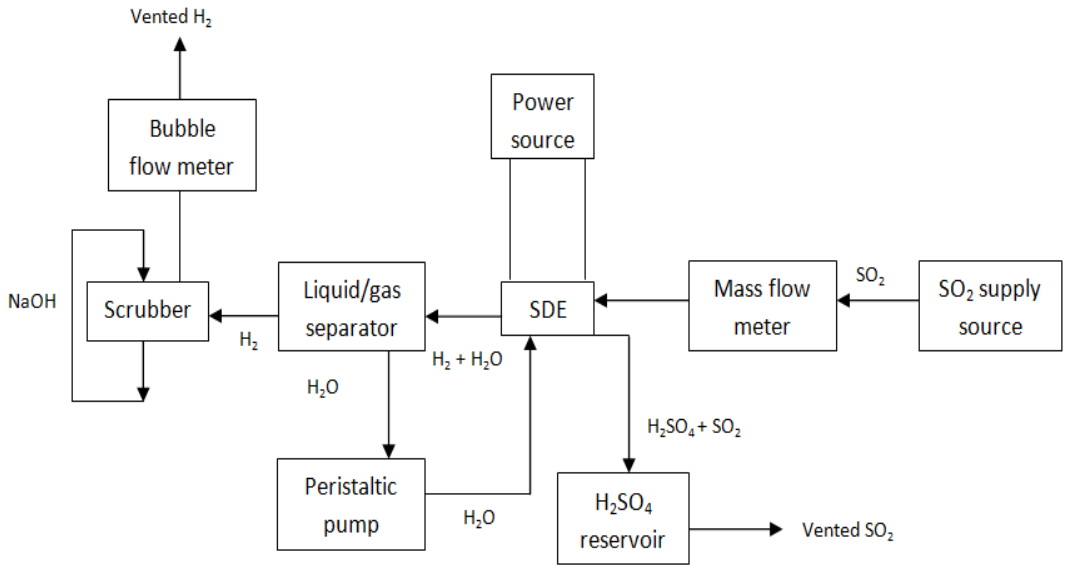

Figure 36: Schematic of test bench lay-out

Figure 37: Photo of the assembled test bench

The SDE requires that deionised water be fed to the cathode and sulphur dioxide be fed to the anode whilst inducing a current over the cell. The DC power supply was a TDK-Lambda GenH 750W model and had two terminals connected over the current collector to provide the electrical energy for electrolysis and serve as the external circuit. The power supply also had two banana plug attachments that were inserted into the bipolar plates in order to measure the cell voltage.

The sulphur dioxide is supplied by a storage tank and its flow rate controlled by a mass flow meter. The liquid/gas separator contains the deionised water for the process, which is circulated through the anode by a peristaltic pump (Watson Marlow 520Du). The produced sulphuric acid is drained to a reservoir whilst the excess sulphur dioxide is vented by the test bench hood. The produced hydrogen gas and circulating water then flowed to the gas/liquid separator. The hydrogen gas is isolated by the separator and travels to a scrubber. The scrubber contains a 25% sodium hydroxide solution (NaOH) that reacts with any sulphur containing gases to produce highly pure hydrogen gas. The hydrogen gas then travels through the bubble flow meter which is used to determine the hydrogen gas production rates, after which the gas is vented by the hood.

5.2 Electrolyzer Integrity

Preliminary testing was done to ensure that the cell functions correctly under the operating conditions set forth for testing the effects of upscaling.

5.2.1 Fluid leakage test

A fluid leakage test was carried out by circulating water through both the anode and cathode side of the cell. The test showed that a leak occurred between the interface of the bipolar plates and the MEA. After inspection of the plates, it was noticed that the GDL's were oversized and that the membrane contained wrinkles which did not deform enough to serve as a gasket between the two bipolar plates. The design had to be altered to facilitate a gasket.

The new modified bipolar plate design (Figure 38) featured a protrusion containing the flow fields on both plates so that gaskets may be inserted on both sides of the MEA.

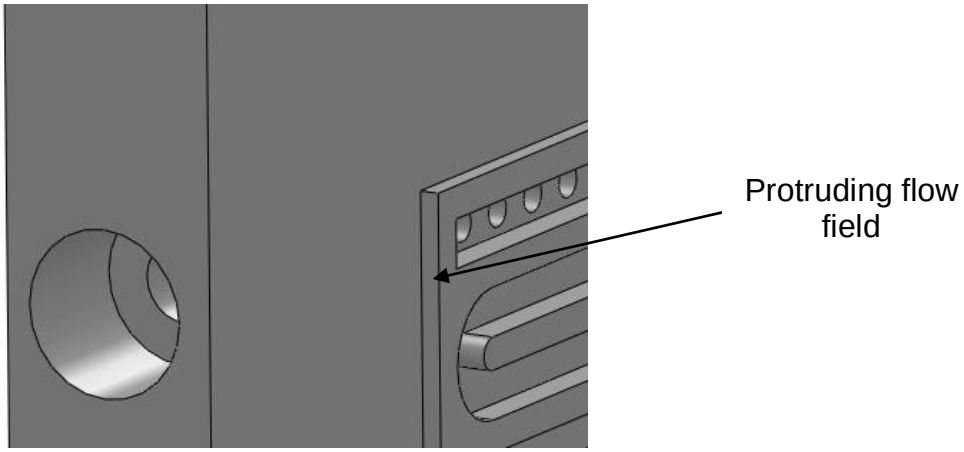

Figure 38: Alteration to bipolar plate design model indicating the protrusion required for the gasket

The gasket required a very good resistance to harsh acids and it was accordingly determined through a literature search that Viton and Hypalon would resist the acids. Hypalon was chosen since a review of its properties indicated that its corrosion resistance is similar to Viton but at a fraction of the cost.

Viton is also less deformable than the Hypalon and may not absorb the minor wrinkles of the membrane or the oversized region of the GDL. The thinnest sheet thickness that could be obtained was 1.5mm

A number compression tests were done on the Hypalon elastomer in order to determine the height of the protrusion as well as the torque that had to be applied to each bolt without damaging the MEA during assembly. The compression test apparatus was a Monsanto Type W Tensometer with an IMP Calibration Services module attached for the digital display of the results. The IMP Calibration Services module plotted the deflection of the elastomer as a function of the applied force. The force was then translated to a normal pressure by noting the following relation:

$$\sigma = \frac{F}{A}$$

where F - Applied force (N)

A - Surface area of the elastomer (m^2)

The normal pressure was then used to calculate the torque necessary to cause the desired deflection. The height of the protrusion was calculated as 1.2mm and each bolt had to be torqued to 4Nm to ensure that the GDL's are right up against the flow channels without any damage caused to the MEA. Further details of the experimental work and calculations are presented in Appendix E.

The bipolar plates were then remanufactured with the gaskets in place and a second leakage test was performed under the same conditions. Testing showed no leaks present, the temperature was then increased to 80°C to establish whether the gaskets would still provide an adequate seal at the operating temperature. The second test showed that the gasket provided an adequate seal against fluid leaks.

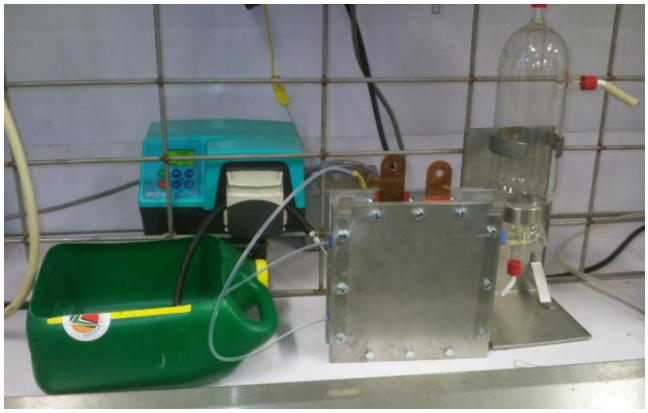

Figure 39: Fluid leakage test set-up showing the electrolyzer coupled with a peristaltic pump and water reservoir in the foreground

5.2.2 Gas leakage test

To determine whether the electrolyzer would seal adequately against gaseous species, a pressure test was performed by connecting the anode and cathode of the cell to a pressurized oxygen supply. The test showed oxygen bubble formation at numerous locations through the bipolar plate, indicating that the graphite was too porous for use as bipolar plates.

Figure 40: Gas leakage test set-up with a pressurized oxygen supply (not shown) coupled to the electrolyzer

In order to overcome this problem, the graphite had to be densified. Electrographite Carbon Co. (Pty) Ltd. supplied phenolic resin impregnated graphite plates that were impermeable to fluids and gases which also met the design requirements. Since new plates were to be manufactured, it was decided to increase the thickness of the plates so that a 1/8" NPT (National

Pipe Thread) holes could be tapped for the inlet and outlet components rather than the previously used M3 ISO threaded holes. The reason being that the PTFE proved to be too flexible as inlet and outlet components and 1/8" NPT PFA (Perfluoroalkoxyethylene) inlet and outlet components could be readily obtained along with PFA tubing, thus eliminating the high cost of producing the custom made PTFE components. The PFA fittings would also withstand the effect of the sulphuric acid and sulphur dioxide.

A second gas leakage test was performed with the new plates and there appeared to be no pressure loss through the cell and no gas bubble formations. This indicated that the cell was air tight. A photo of the Hypalon gasket is shown in Figure 41.

Figure 41: Photo of Hypalon gasket

As an additional test, two different types of graphite were used to manufacture the bipolar plates in order to determine whether the orientation of the graphite's electrical conduction planes will influence the cells performance. The phenolic resin impregnated isostatically (Isos) press-formed graphite plates and isotropically (Isot) press-formed graphite plates were procured and machined by Electrographite Carbon Co. (Pty) Ltd. The difference between the plates is that the isostatically press-formed plates will only conduct electrons in the plane perpendicular to the current collector, whilst the isotropically press-formed plates are orthotropic in nature and would conduct electrons in every direction.

5.3 Membrane Preparation Procedure

In the dehydrated state the proton exchange membranes do not have the proton conduction ability necessary for the electrolysis process. The hydrophobic properties of the MEA were determined by pouring water over the MEA and performing a visual inspection. If the water seamlessly flows off the MEA, it is an indication that the membrane is too dehydrated, if the water is absorbed into the MEA or the MEA has a wet appearance, it is an indication that it is hydrated. From previous experiences, MEA's generally had to be hydrated with water for a couple of hours at ±40°C for them to become fully hydrated and function correctly. The temperature may be gradually increased to 80°C to ensure full hydration. After the membranes were hydrated, the electrolyzer was assembled.

5.4 Electrolyzer Preparation

To prevent possible detrimental chemical reactions taking place within the cell, the anode side was purged with 80ml/min of nitrogen gas whilst flushing water through the cathode side for 15 minutes to eliminate impurities. Nitrogen was used for purging since it is very chemically inert [14]. After the cell was purged with nitrogen, it was purged with 80ml/min of hydrogen gas to remove the nitrogen and saturate the bipolar plates.

5.5 MEA Hydrogen Pump Test

The MEA's were tested to determine whether they are conducting the hydrogen protons necessary for electrolysis. Tests were conducted by applying a current over the cell whilst circulating only hydrogen gas through the anode and water through the cathode. The hydrogen gas is oxidized to form hydrogen protons (H^+) and electrons (e^-). The electrons will be conducted to the cathode by means of the external circuit. If the H^+ are conducted through the membrane and reduced to hydrogen gas at the cathode, the membrane is conducting the hydrogen protons and functioning correctly.

The steps that were followed in performing the hydrogen pump test were conceptualized from previous experiences and are as follows:

1. The heating pad temperature was set to 80ºC by means of the relay and thermocouple sub-system. The cell was then left until the flow fields reached the 80ºC operating temperature whilst circulating the water through the cathode. As soon as the operating temperature was reached, the hydrogen gas was introduced at the anode with a flow rate of 500ml/min.
2. A constant current of 0.5A was applied over the electrolyzer until the cell voltage stabilized. As soon as the cell voltage stabilized, the current and cell voltage readings were taken.
3. The current was then incrementally increased by 0.5A until a cell voltage of 1.4V[d] was reached, waiting for the cell voltage to stabilize at each increment and noting the current and cell voltage values.

Two 5-layer MEA's were tested during the hydrogen pump test. It was noticed during testing of the first MEA that the voltages were extremely high for the applied currents. It was also noticed before testing that the membrane showed an odd discoloration (Figure 42). Although the membrane performed very poorly, hydrogen was produced during the test.

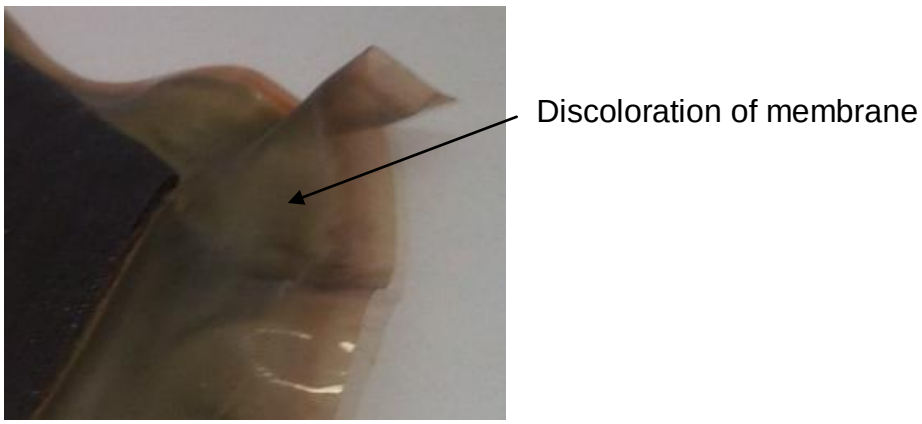

Figure 42: Discoloration of the 1st membrane

[d] Higher voltages will cause severe degradation of the GDL's.

The second membrane showed much more promising results (Table 5), with much lower cell voltages at the applied currents and was used to perform the subsequent tests.

Table 5: Variation of the cell voltage as a function of the induced current as obtained from the hydrogen pump tests for the MEA's tested

Applied current (A)	Cell voltage (V)	
	1st MEA	2nd MEA
1	0.04	0.02
2	0.09	0.05
3	0.15	0.07
4	0.19	0.09
5	0.24	0.11
6	0.3	0.14
7	0.34	0.16
8	0.39	0.18
9	0.45	0.2
10	0.51	0.23

The results obtained from the hydrogen pump tests were used to construct a polarization curve (Figure 43). The increased cell voltage of the 1st membrane is clearly illustrated by the curve. It should be noted that the fluid- and gas leakage tests were performed with the 1st MEA present in the cell.

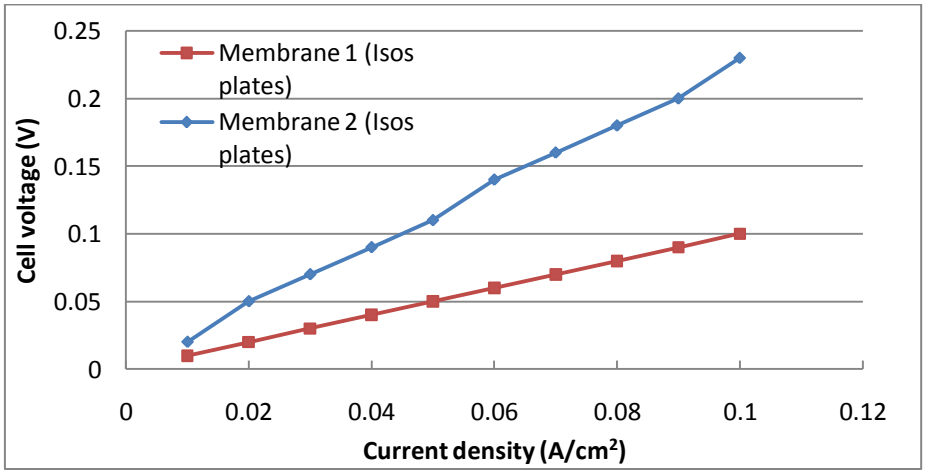

Figure 43: Polarization curves of the hydrogen pump test using the isostatically press-formed bipolar plates

One possible reason that the 1st MEA performed so poorly could be due to the formation of iron oxide (Fe_2O_3, rust) on the bolts and aluminium oxide (Al_2O_3) on the back plates during the fluid leakage test. The iron oxide and aluminium oxide were then introduced onto the SDE by the circulating water. The odd discoloration of the membrane (Figure 42) can also be contributed to the rust precipitation. Scanning Electron Microscopy (SEM) analyses were performed on both the membranes to investigate to poor performance of the 1st MEA, with the 2nd MEA serving as a reference. The SEM analysis showed that there were unusual high amounts of Fe and Al present on the 1st MEA, thus supporting the hypothesis that the oxides could have contributed to the poor performance of the membrane. The results of the SEM elemental analysis are indicated in Table 6. The increased silicon (Si) and carbon (C) content in the 1st MEA is most likely due to the fact that silicon carbide (SiC) sanding paper was used in preparing the specimen for the SEM analysis.

Table 6: Elemental analysis on the 1st MEA and 2nd MEA

Element	Weight %	
	1st MEA	2nd MEA
C	70.05	67.4
F	25.57	29.08
Mg	0.12	0.13
Al	0.75	0.29
Si	1.24	0.5
Ca	0.3	0.33
Fe	0.48	0
Pt	0.54	0.53
Na	0	0.16
S	0.96	1.58
Total	100	100

5.6 Electrical Resistance of the Cells

The electrical resistance of the 25cm^2 cell and the 100cm^2 cell with the isostatically press-formed graphite plates and isotropically press-formed graphite plates were measured across the bipolar plates using a Hewlett Packard 4328A milli-ohmmeter with the MEA present. The measurements were taken at atmospheric conditions with no fluids present.

The isostatically press-formed plates had an electrical resistance of 22.5 mΩ whilst the isotropically press-formed plates had a resistance of 52 mΩ, the resistance of the 25cm^2 cell was measured as 13 mΩ. These resistances were measured since they will influence the required cell voltage necessary for electrolysis.

5.7 Testing Procedure Applied to the 25cm^2 and 100cm^2 Cells

The test procedure for testing the electrolyzer was designed using previous experience and was performed as follows:

1. The heating pad temperature was set to 80ºC by means of the relay and thermocouple sub-system. The cell was then left until the flow fields reached the 80ºC operating temperature whilst circulating water through the cathode.
2. The anode compartment was flushed with SO_2 gas for 2 minutes to ensure SO_2 saturation. This was necessary to remove any undesirable chemical species which may be present.
3. A continuous flow of SO_2 was then delivered to anode at a flow rate of 500ml/min whilst the deionised water was circulated through the cathode at 150ml/min.
4. A constant current of 0.5A was applied over the cell. The current and cell voltage readings were taken as soon as the cell voltage stabilized, this was usually in the region of 3min.
5. The current was then incrementally increased by 0.5A, noting the cell voltage at each increment. A bubble flow meter was used to determine the hydrogen gas production rate at each increment. The production rates were measured a few minutes after the cell voltage stabilized, since the produced hydrogen gas at the specific increment still had to travel to the bubble flow meter.

After the first test was completed, the SDE was disassembled and inspected. Severe sulphur precipitation was present in the PFA tubing (Figure 44) and on the cathode side of the MEA when the 100cm^2 cell was tested. Higher concentrations of the precipitate were present at the outlet (Figure 45). The

precipitated sulphur present on the MEA was gently cleaned off by using a clean cloth and deionised water whilst the tubing was cleaned by increasing the deionised water flow rate and tapping the tubing in order to dislodge the sulphur. The MEA and tubing were cleaned before performing subsequent tests.

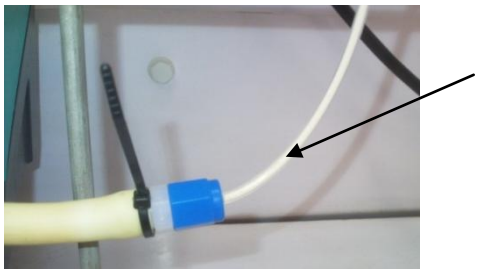

Figure 44: Sulphur precipitate in PFA tubing

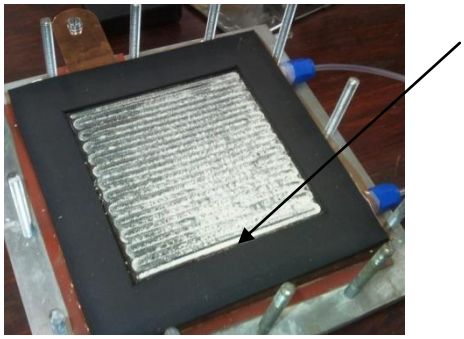

Figure 45: Sulphur formation on the cathode side

The 100cm^2 cell was tested twice with the isostatically press-formed bipolar plates and twice with the isotropically press-formed bipolar plates with the results presented in Table 7 and
Table 8, respectively.

Table 7: Results obtained testing the 100cm^2 cell with the 2nd MEA and the *isostatically* press-formed bipolar plates during test 1(left) and test 2 (right)

Test 1			Test 2		
I (A)	**Cell voltage (V)**	**Hydrogen production rate (l/h)**	**I (A)**	**Cell voltage (V)**	**Hydrogen production rate (l/h)**
0.5	0.33		0.5	0.47	
1	0.4		1	0.56	
1.5	0.47		1.5	0.64	
2	0.52		2	0.72	
2.5	0.58		2.5	0.83	
3	0.64		3	0.94	
3.5	0.75		3.5	1.01	
4	0.8		4	1.04	0.95
4.5	0.85	1.33	4.5	1.08	1.34
5	0.92	1.72	5	1.11	1.64
5.5	0.99	2.73	5.5	1.13	1.99
6	1.08	2.67	6	1.16	2.17

Table 8: Results obtained testing the 100cm^2 cell with the 2nd MEA and the *isotropically* press-formed bipolar plates during test 1(left) and test 2 (right)

Test 3			Test 4		
I (A)	Cell voltage (V)	Hydrogen production rate (l/h)	I (A)	Cell voltage (V)	Hydrogen production rate (l/h)
0.5	0.56		0.5	0.56	
1	0.69		1	0.68	
1.5	0.8		1.5	0.78	
2	0.87		2	0.85	
2.5	0.93		2.5	0.91	
3	1.01		3	0.98	
3.5	1.07		3.5	1.03	
4	1.12	0.86	4	1.11	0.96
4.5	1.17	1.15	4.5	1.14	1.42
5	1.2	1.63	5	1.16	1.77
5.5	1.24	1.89	5.5	1.2	2.08
			6	1.24	2.23

The 25cm^2 cell was tested once with no alterations to the bipolar plates and the results are presented in Table 9.

Table 9: Results obtained from testing of the 25cm^2 cell

I (A)	Cell voltage (V)	Hydrogen production rate (l/h)
0.5	0.14	
1	0.28	
1.5	0.38	
2	0.47	
2.5	0.55	
3	0.57	
3.5	0.59	
4	0.61	
5	0.64	1.47
6	0.68	1.58
7	0.72	2.29
8	0.76	2.38
9	0.8	2.74
10	0.84	3.42
11	0.89	3.61
12	0.94	3.56
13	0.99	3.54
14	1.05	4.12
15	1.12	3.99
16	1.18	3.57

5.8 Summary

Chapter 5 addressed the experimental set-up and procedure used for testing the effects of upscaling the SDE. The lay-out of the test bench and its operation was addressed. Preliminary testing of the SDE showed fluid leakage between the bipolar plates and MEA and gas leakage through the bipolar plates. This was corrected by using Hypalon gaskets and using phenolic resin impregnated graphite bipolar plates. The electrical resistances of the cells were measured over the bipolar plates indicating that the resistance of the 25cm^2 cell was the lowest at 13 mΩ, followed by the 100cm^2 cell equipped with the isostatically press-formed graphite plates at 22.5 mΩ and the 100cm^2 cell equipped with the isotropically press-formed graphite plates at 52 mΩ, respectively. Testing of the 100cm^2 cell indicated a severe sulphur precipitation that had to be cleaned before performing subsequent tests.

6 DISCUSSION

6.1 Sulphur Precipitation

Significant amounts of sulphur were produced at the cathode during testing of the 100cm^2 cell which adhered to the MEA and the bipolar plate. The sulphur was formed from the reduction of sulphur dioxide when it crosses the membrane:

$$SO_2 + 4e^- \rightarrow S + O_2$$

The sulphur also precipitated in the test bench tubing, restricting the fluid flow causing a detrimental back pressure. The increased pressure drop induced by the serpentine flow channels could have promoted the crossover of sulphur dioxide to the cathode. The pressure drop also caused significant amounts of sulphur to accumulate at the outlet of the cathode bipolar plate (Figure 45). The sulphur precipitate was also indentified in the SEM analysis (Table 6) with an increase of 0.62 wt% S when compared to the 1st MEA (which was not exposed to SO_2). The sulphur formation at the cathode would increase the voltage necessary for electrolysis by contaminating the catalyst layer and will also increase the cells resistance by covering the electrode [27]. The sulphur precipitate may be reduced by increasing the cathode pressure or decreasing the anode pressure, thus limiting the crossover of SO_2 to the cathode. The 25cm^2 cell exhibited no sulphur precipitation during testing. Development of MEA's impermeable to SO_2 crossover will greatly increase the feasibility of the SDE.

6.2 Testing of the 100cm^2 Cell

The 1st test of the 100cm^2 cell was conducted with the *isostatically* press-formed bipolar plates and the 2nd MEA (Figure 46).

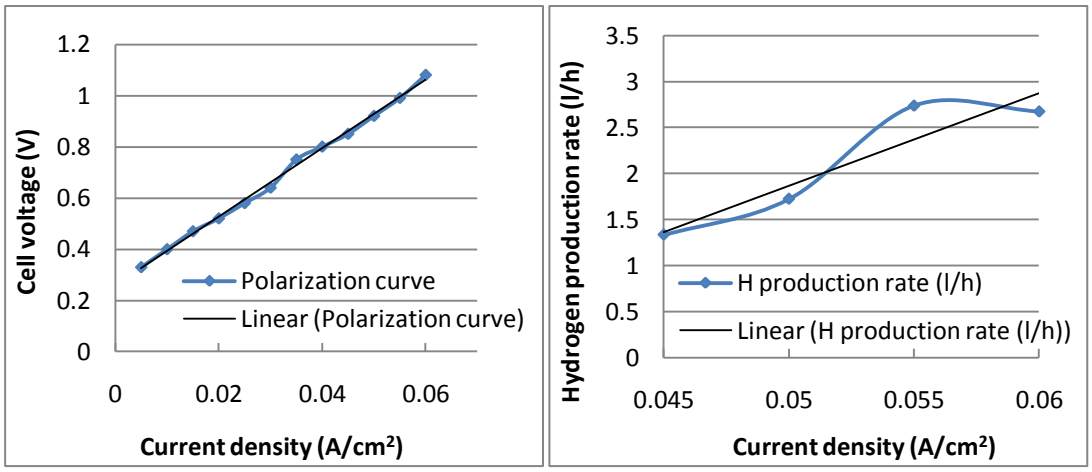

Figure 46: Polarization curve (left) and hydrogen gas production rate vs. current density (right) of test 1 using the 2nd MEA with isostatically press-formed graphite bipolar plates

Hydrogen gas production started at a current density of 0.045A/cm^2 and a cell voltage of 0.85V. The production rate was measured as 1.33 l/h which increased to a rate of 2.67 l/h at a current density of 0.06A/cm^2 and cell voltage of 1.08V. The current was then increased to 6.5A after which the cell voltage increased beyond the 1.4V limit when further testing was aborted due to reason previously discussed. Figure 46 also indicates a linear trendline for the hydrogen production rate.

The 2nd test was also conducted with the *isostatically* press-formed graphite bipolar plates and the 2nd MEA. The polarization curve and hydrogen production rate vs. current density curve are presented in Figure 47.

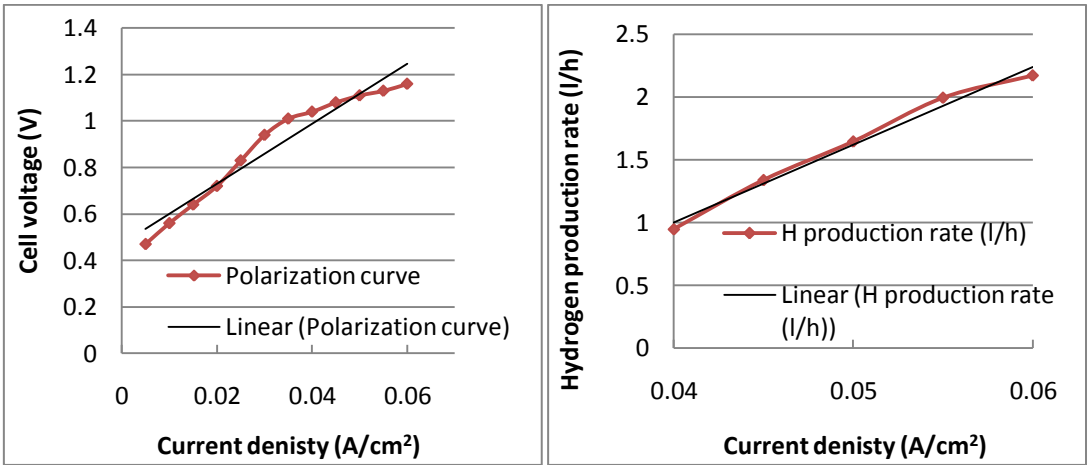

Figure 47: Polarization curve (left) and hydrogen gas production rate vs. current density (right) of test 2 using the 2nd MEA with isostatically press-formed graphite bipolar plates

During this test the hydrogen gas was produced at a current density of 0.04A/cm^2 with a corresponding cell voltage of 1.04V. The production rate was measured as 0.94 l/h which increased to 2.16l/h at a current density of 0.06A/cm^2 and a cell voltage of 1.16V. The current was subsequently increased to 6.5A after which the cell voltage increased beyond the 1.4V limit when further testing was halted.

The 3rd test was conducted by using the *isotropically* press-formed graphite bipolar plates along with the 2nd MEA and the results are illustrated in Figure 48.

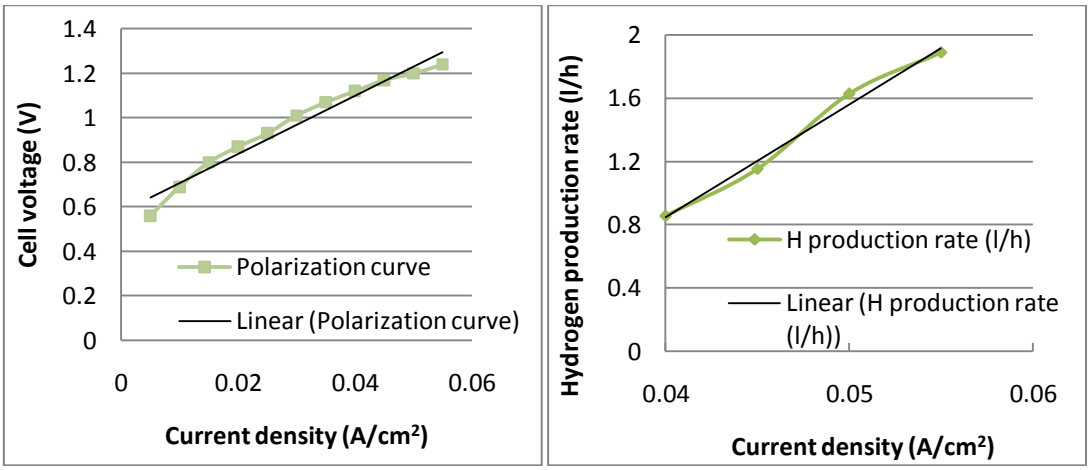

Figure 48: Polarization curve (left) and hydrogen gas production rate vs. current density (right) of test 3 using the 2nd MEA with isotropically press-formed graphite bipolar plates

A hydrogen gas production rate of 0.85 l/h was noted at current density of 0.04A/cm^2 and a cell voltage of 1.12V. The production rate increased to 1.88 l/h at a current density of 0.055A/cm^2, corresponding to a cell voltage of 1.24V after which the testing was aborted due to the reasons already discussed.

The 4th test was conducted with the *isotropically* press-formed graphite plates along with the 2nd MEA (Figure 49).

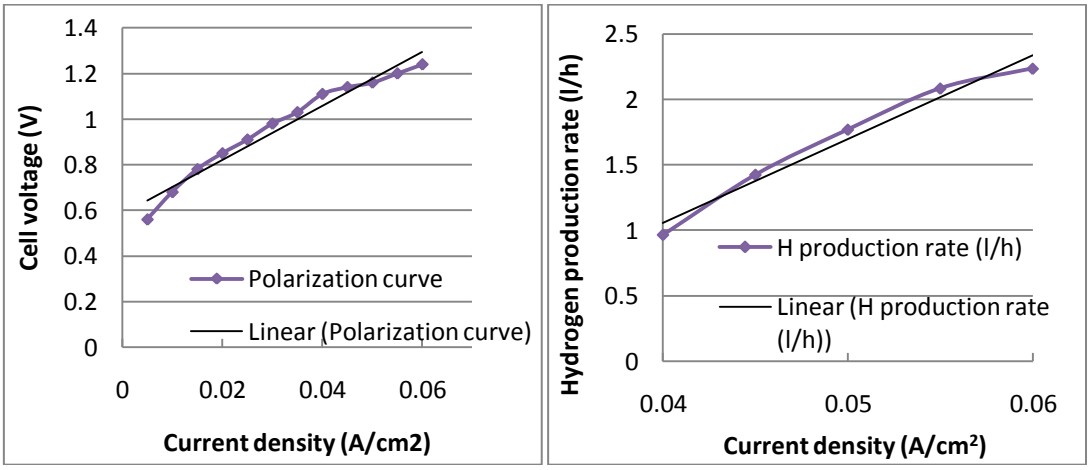

Figure 49: Polarization curve (left) and hydrogen gas production rate vs. current density (right) of test 4 using the 2nd MEA with isotropically press-formed graphite bipolar plates

A hydrogen gas production rate of 0.96 l/h was observed at a current density of 0.04A/cm^2 and a corresponding cell voltage of 1.11V. Testing was halted at a cell voltage of 1.24V and a current density of 0.06A/cm^2, the hydrogen production rate at this voltage was measured as 2.23 l/h.

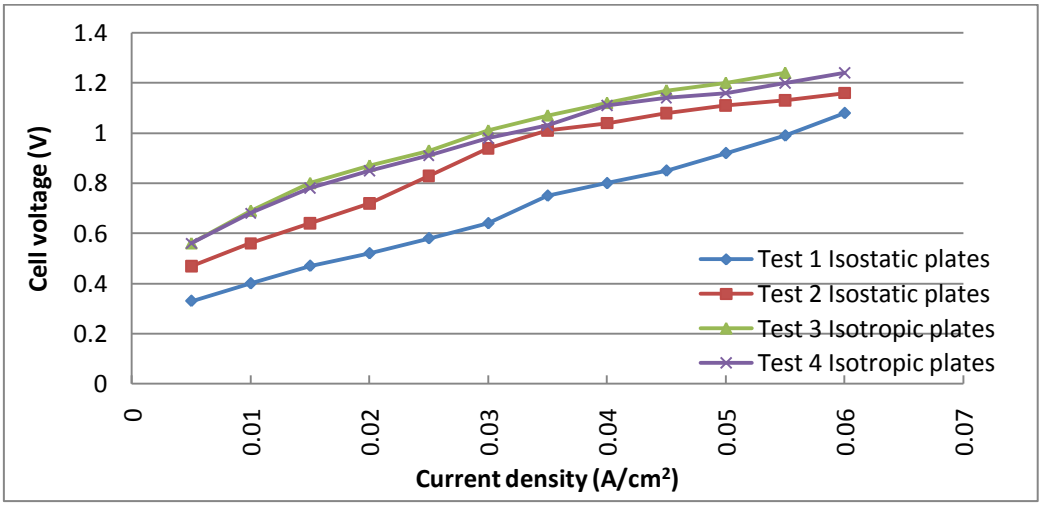

Figure 50: Polarization curves of the isostatic- and isotropically press-formed graphite bipolar plates with the 2nd MEA

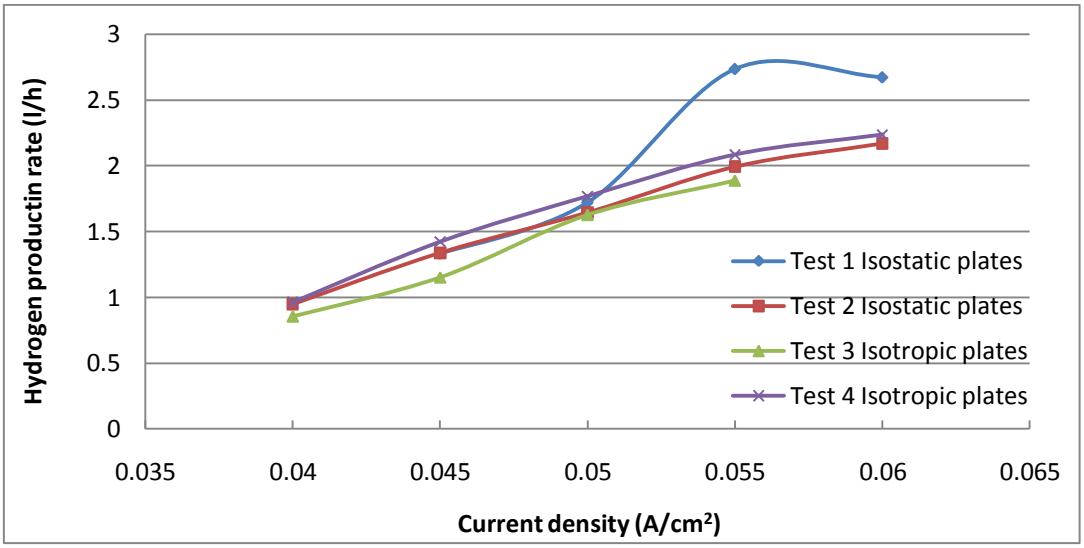

Figure 51: Hydrogen gas production rate vs. current density of isostatic- and isotropically press-formed graphite bipolar plates

The polarization curves and hydrogen production rates vs. current densities for the 100cm^2 cell are illustrated in Figure 50 and Figure 51, respectively. It can clearly be noted that an increase in the induced current leads to an increase in the hydrogen production rates.

The 1st test with the isostatically press-formed graphite bipolar plates shows much lower cell voltages at the applied currents than the subsequent tests. The lower cell voltage illustrates that a lower electrical energy input is required for electrolysis. The 1st test also shows higher hydrogen production rates for higher values of current density. This better performance can be attributed to the fact that the membrane was not previously contaminated by the formation of sulphur at the cathode and is not necessarily an indication of greater performance of the isostatically press-formed graphite plates.

The 2nd test with the isostatically press-formed bipolar plates indicates that a decreased performance with higher cell voltages is required for electrolysis at the same induced currents than the previous test. The second test also indicates a reduced hydrogen production rate. This decreased performance can be attributed to the contamination of the catalyst by the precipitated sulphur, the precipitation of sulphur on the bipolar plates and the oxidation of the carbon containing GDL;s due to excessive cell voltages.

The 3rd and 4th tests made use of the isotropically press-formed bipolar plates and both tests had nearly identical results in terms of their polarization curves and hydrogen production rates vs. current density. The isotropically press-formed bipolar plates did show a slight increase in cell voltages when compared to the 2nd test. This slight increase can also be attributed to the oxidation of the carbon containing GDL's and the effects of the sulphur precipitation. The 1st, 2nd and 3rd tests exhibit only a slight variation in hydrogen production rates. It is thought that this slight variation could be due to human error, since the production rates calculated for the 2nd test falls between the production rates measured for the 3rd and 4th tests.

From the above discussion it cannot be definitively concluded that the electrical conduction planes in the bipolar plates will influence the performance of the electrolyzer. A major drawback was identified, that being the use of carbon supports in the GDL's. The GDL's place a limit on the cell voltage due to the oxidation of carbon and since the cell voltage and hydrogen production rates are proportional it also limits the hydrogen production rates.

6.3 Testing of the 25cm^2 Cell

The commercially acquired 25cm^2 cell was only tested once, Figure 52 illustrates the polarization curves as well as the hydrogen production rates vs. the current densities obtained.

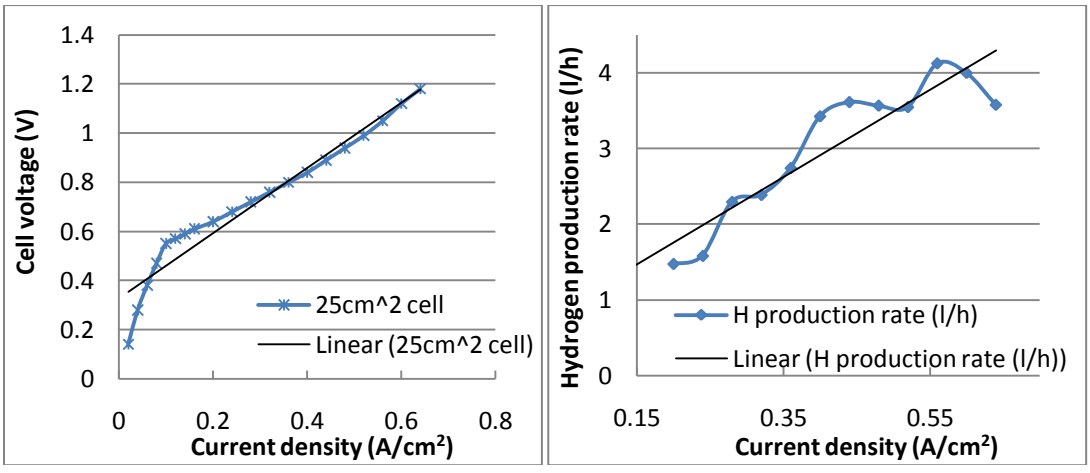

Figure 52: Polarization curve (left) and hydrogen production rate vs. current density (right) of a commercially acquired 25cm^2 cell

Hydrogen production began at a cell voltage of 0.64V and current density of 0.02A/cm^2, which was the in the expected range as identified in the literature [8]. The production rate at the induced 0.64V was determined as 1.47 l/h and reached a maximum value of 4.12 l/h at 1.05V, after which it decreased to 3.57 l/h at a current density 0.64A/cm^2 and cell voltage of 1.18V.

The clear difference in the slope of the polarization curve between 0-0.1A/cm^2 and 0.1-0.65A/cm^2 can be attributed to the degradation of the carbon containing GDL's. As previously discussed, the initial degradation of the carbon electrodes are substantially more during the first couple minutes of testing, after which it decreases and levels out (see 2.2.4 Gas diffusion layer and catalyst layer).

It was also noted during tests that the hydrogen production rates are more erratic and began to decline after a cell voltage of 1.05V and current density of 0.6A/cm^2 was reached (Figure 52, right). This erratic production rates could however not be explained but it is possible that it resulted from human error in measuring the hydrogen gas production rates.

6.4 Comparison between the 25cm^2 and 100cm^2 Cell

One of the main disadvantages of the 100cm^2 cell is the low current densities that were achievable before the cut off voltage of 1.4V was reached. The maximum current density out of all the tests was determined as 0.06A/cm^2 whilst the 25cm^2 could achieve current densities in excess of 0.6A/cm^2.

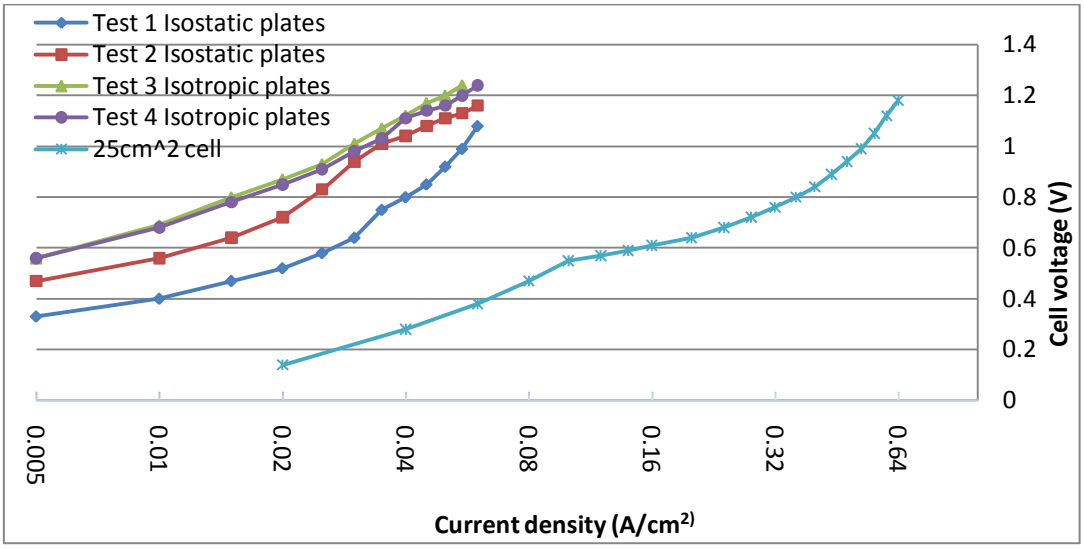

Figure 53: Polarization curves of the 100cm^2 cell and 25cm^2 cell[e]

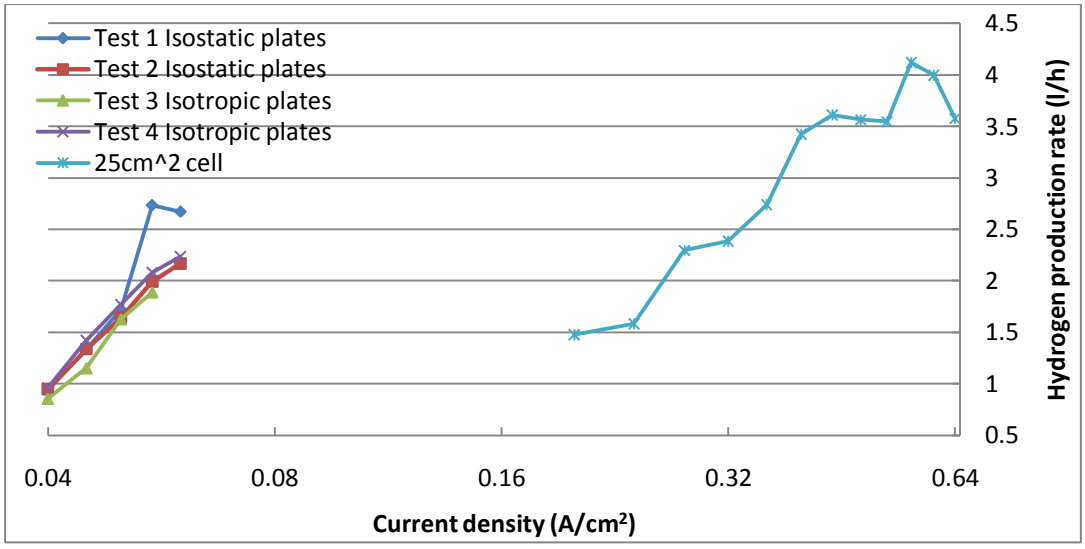

Figure 54: Hydrogen production rates vs. current density of the 100cm^2 cell and 25cm^2 cell[e]

The reasons that higher current densities, and thus greater utilization of the reaction area could be achieved by the 25cm^2 cell, is thought to be due to the smaller active area of the cell and the cells lower electrical resistance as compared to those of the 100cm^2 cell.

[e] It should be noted the Current density axis has a logarithmic scale

Ohm's law states that:

$$V = IR$$

where V - Cell voltage (V)
I - Induced current (A)
R - Electrical resistance of the cell (Ω)

Assuming a cell voltage of 1.4V and an electrical resistance value as determined in §5.6, it was calculated that the theoretical maximum current induced in the 25cm^2 cell and 100cm^2 cell would be 107.69A and 62.22A, respectively. This translates to a theoretical maximum current density of 4.3A/cm^2 for the 25cm^2 cell and 0.62A/cm^2 for the 100cm^2 cell therefore indicating that a smaller active area can achieve greater reaction kinetics. These theoretical values will not be achievable for two reasons:

- The cells resistances were measured under dry conditions with no reactants or products present.
- The cell voltage measurements were taken across the bipolar plates, and not across the current collector over which the current is induced to conform to the common practice in fuel cell and electrolyzer testing.

Apart from the 25cm^2 cell having a lower electrical resistance due to its material composition, it will also have a lower electrical resistance due to its smaller internal volume for reactant/products when compared to the 100cm^2 cell, thereby reducing the required cells voltages.

Another advantage of the high current densities achieved by the 25cm^2 cell is that high current densities lead to a decrease in SO_2 crossover to the cathode. Staser *et al.* (2009) concluded that an increase in the current density will lead to an increase in water flux into the membrane thereby decreasing SO_2 crossover to the cathode. The SO_2 crossover is reduced since the SO_2 will dissolve into the water. This was evident during testing since no SO_2 seemed to crossover to the cathode with the 25cm^2 cell.

The hydrogen production rate of the 25cm^2 cell was also higher than that of the 100cm^2. The increased production rates can also be attributed to the higher current densities achieved by the 25cm^2 cell.

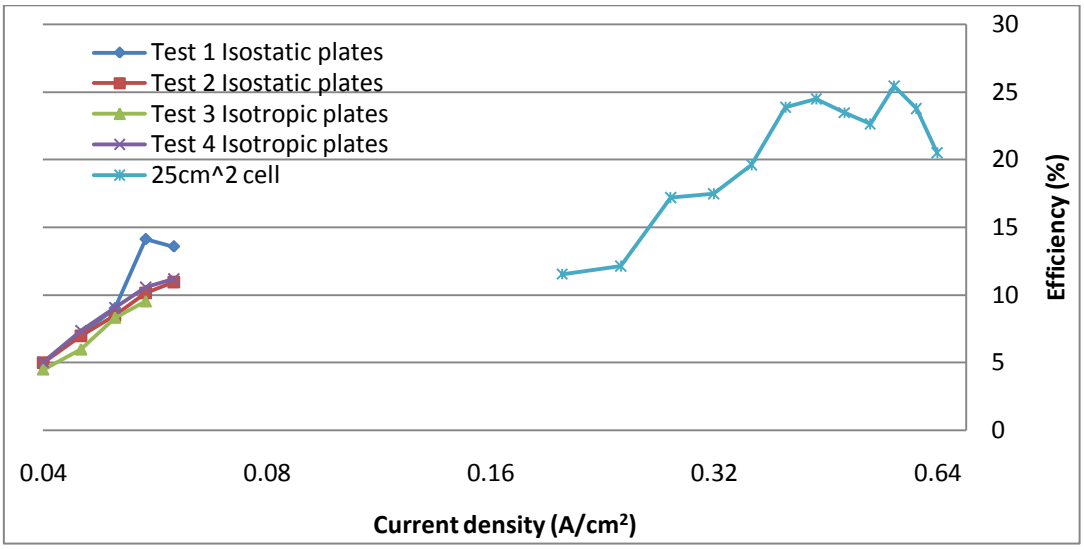

Figure 55: Electrolyzer efficiency vs. current density[f]

The efficiencies of the 25cm^2 cell and 100cm^2 cell were determined, as based on engineering practise, by only considering the heat energy input required by the heating pad and the electrical energy required for electrolysis[g]. The equation used for determining the efficiency was as follows:

$$\eta = \frac{energy\ contained\ in\ produced\ H_2}{heat\ energy + electrical\ energy}$$

Based on the data of Figure 55, it was deduced that the 25cm^2 cell could achieves a much higher efficiency than the 100cm^2 cell. The higher efficiency is attributed to the lower cell voltage due to the lower electrical resistance of the 25cm^2 cell and the fact that the cell only makes use of a 40W heating element. The maximum efficiency achieved by the 100cm^2 cell was determined as 13.6% whereas the 25cm^2 cell could achieve efficiencies of as much as 25%. Details of determining the cell efficiencies are addressed in Appendix F.

[f] It should be noted the current density axis has a logarithmic scale

[g] It should be noted that the electrical energy was calculated by considering the current induced through the current collector and the voltage measurements across the bipolar plates and will thus only serve for comparative purposes in this particular study.

After testing of the 100cm^2 cell and 25cm^2 cell were completed, the results were compared with those found in the literature. However, the literature does not discuss the geometry of these electrolyzers and the testing parameters vary which make comparison of the results very difficult.

The results that were obtainable are from the Proton Energy Systems (PES) cell and another cell constructed by The University of South Carolina (USC). The PES cell was built as a three cell stack assembly with an active area of 86cm^2 and a Pt loading of 4mg/cm^2. It was constructed from Hastelloy B and Teflon wetted parts with porous titanium electrodes. The USC cell was constructed from much of the same materials as the cells tested in this study. It was comprised of a Nafion 115 membrane, carbon paper electrodes and carbon paper flow fields along with graphite back plates. It had an active area of 40cm^2 and a Pt loading of 0.5mg/cm^2.

The PES and USC cells were tested with the SO_2 gas dissolved in a 30wt% H_2SO_4 solution. This already promotes the cells performance since the solution reduces the required cell voltage necessary for electrolysis. The reason for not dissolving the SO_2 in H_2SO_4 during this study is that it was not evident during the experimental phase that the other cells made use of this method.

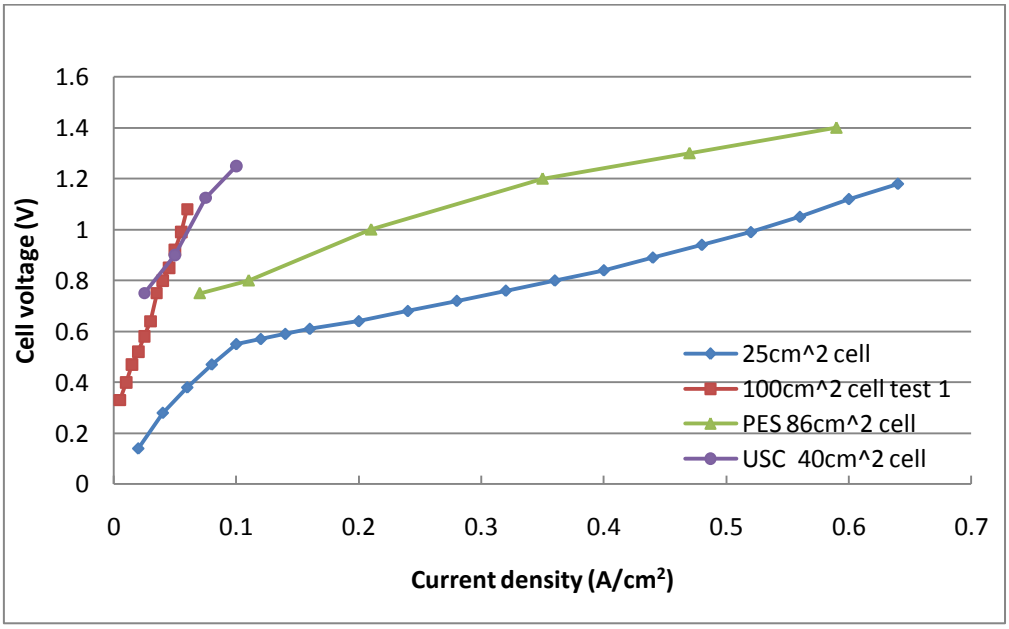

Figure 56: Polarization curves of the 100cm^2 cell, the 25cm^2 cell, the PES and USC cells

The polarization curves of the best result of the 100cm^2 cell, as well as the 25cm^2 cell and the PES and USC cells are illustrated in Figure 56. The USC cell and 100cm^2 cell showed very similar results, which were both quite poor. The USC cell did however reach higher current densities than the 100cm^2 cell before the voltage limit was reached, this is most likely attributed to the reduced cell voltage caused by dissolving the SO_2 in the 30%wt H_2SO_4 solution. However, the 25cm^2 cell showed much greater performance than the USC cell without the introduction of the 30wt% H_2SO_4.

The PES cell showed much better performance than the 100cm^2 with nearly as high current densities achievable as that of the 25cm^2 cell at only slightly higher voltages. The reason that the PES cell could achieve nearly the same current densities as the 25cm^2 cell, even though it has a much greater surface area, can be attributed to the materials used to construct the cell, the high catalyst loading as well as the introduction of SO_2 and 30wt% H_2SO_4 solution. Although it seems that the PES cell configuration would be the most favourable in terms of production quantities, a major disadvantage was that it only lasted a few tests, due to the internal corrosion. Another major disadvantage was the high catalyst loading which makes production extremely expensive.

6.5 Corrosion

One of the main advantages of the 100cm^2 cell and 25cm^2 cell is that there was no evidence of corrosion. With the Proton Energy Systems cell, testing had to be aborted due to the degradation of the titanium electrodes after only a few experiments [8]. A visual inspection revealed that none of the components or test bench equipment had been corroded by the sulphuric acid.

6.6 Conclusions

From the above discussion, the following conclusions are made:

- The materials used in the $100cm^2$ and $25cm^2$ cells showed no degradation due to corrosion in the acid environment making these materials promising candidates for SO_2 electrolysis.

- The different type of conduction planes within the isostatically- and isotropically pressed graphite plates did not seem to influence the performance of the electrolyzer.

- The $100cm^2$ cell showed decreased performance due to the severe sulphur precipitation. The sulphur precipitation can be attributed to the following:
    - The pressure drop caused by the increased length of flow channels which promotes SO_2 crossover to the cathode.
    - The reduced current densities caused by the larger reaction area increasing the probability of SO_2 crossover.

- The $25cm^2$ cell has a much lower electrical resistance than the $100cm^2$ cell. This resulted in higher current densities being achieved and lower cell voltages required for electrolysis. The lower electrical resistance can be attributed to the following:
    - The bipolar plates used to construct the $25cm^2$ cell exhibited a much lower electrical resistance than the plates used to construct the $100cm^2$ cell. This is attributed to the graphite used to produce the plates.
    - The $25cm^2$ cell has a smaller active area and smaller internal volume for reactants and products, thus reducing the cell specific resistance.

- Incorporation of the U-bends did decrease the pressure drop through the flow channels. Although the pressure drop was only slightly decreased, the machining cost may dramatically be decreased, thus it should be taken into account in producing units for further research work or mass production.

To summarize, the 25cm^2 cell was much more efficient than the 100cm^2 cell, it showed higher hydrogen production rates at lower cell voltages than the 100cm^2 cell. The greater performance exhibited by the smaller cell is mainly due to the higher current densities and thus better reactions kinetics achievable due to the smaller reaction area. Smaller cells also have the advantage of not suffering from the *severe effects of sulphur precipitation* and are thus a much more viable option for mass production of hydrogen gas. *Thus it is concluded that creating stack assemblies will prove to be more efficient than linearly upscaling the active area of the electrolyzer.*

6.7 Design Improvements

6.7.1 Decreasing the pressure drop

A possible method to reduce the pressure drop from the inlet to the outlet and across the MEA is by using fewer bends and longer straight sections of flow channels to achieve the same active area. The use of U-bends did prove to be advantageous and should be incorporated into future designs. Other possible features that could reduce the pressure drop include using another inlet, as to divide the bipolar plate into two flow fields.

6.7.2 Decreasing the cells resistance

Apart from using smaller MEA's to decrease the cells resistance, it was noticed that there exists a contact resistance between the current collector and bipolar plates. The resistance can be lowered by using a highly electrically conductive paste or carbon powder between the interface of the current collector and bipolar plates. The reason for opting for a paste or

powder is that it will minimize the amount of air pockets between the two interfaces and lower the cells contact resistance.

It is thought that using channels with a greater contact area with the GDL's and a smaller channel depth might reduce the Ohmic loss term by decreasing the length through which the current is to be conducted. This will lower the electrical resistance of the fluids and decrease the cells resistance. A possible disadvantage of using shallower channels will be that of clogging due to the sulphur precipitate. Using thinner MEA's will have the same effect by decreasing the distance between the bipolar plates thereby reducing the Ohmic losses.

6.7.3 Alteration to test bench

In measuring the hydrogen gas production rates it was assumed that all the gas travelling through the bubble flow meter was hydrogen gas. It was expected that due to the geometry of the liquid/gas separator and the testing procedure that this was a valid assumption. This assumption may not always be valid and therefore the gas/liquid separator should be equipped with an oxygen vent to prevent possible faulty measurement.

6.8 Suggestions for Further Research

The current density, and thus reaction tempos are currently limited by the use of carbon containing GDL's. To increase the efficiency of the SDE, research must be conducted on finding or manufacturing other possible materials or alloys which can withstand the sulphuric acid environment as well as the applied cell voltage required by the cell.

It is also suggested that the various types of methods used to create stack-assemblies should also be investigated i.e. determine the effects of connecting cells in different electrical configurations such as in series, parallel and creating a stack where each cell has its own power source.

The current practice employed in electrolyzer testing is done by inducing an electric current over the current collectors. It is thought that this method is flawed. The induced current will cause an excess amount of electrons to be present at the cathode, thus increasing the possibility of sulphur formation. In the real world application of electrolyzers, a voltage difference will be applied over the cell, thus further testing should be done by varying the applied voltage over the cell and not inducing an electric current.

6.9 Summary

Chapter 6 discussed the results of the study. Neither the 25cm^2 cell nor 100cm^2 cell showed any sign of corrosion due to the acid environment which makes the material used possible candidates for further development of the SDE.

From this study it cannot be definitively proven that the orientation of electrical conduction planes within the isostatic- and isotropically press-formed graphite plates influenced the performance of the SDE.

The 25cm^2 cell exhibited much greater performance when compared to the 100cm^2 cell. The greater performance can be attributed to the higher current densities that were achievable. Higher current densities could be achieved due to smaller reaction area of the cell and the lower electrical resistance of the cell. The high current densities and lower pressure drop of the 25cm^2 cell also resulted in no SO_2 crossing over to the cathode.

It was thus concluded that using more cells with smaller active areas will be much more efficient than linearly upscaling an electrolyzer.

7 REFERENCES

[1] [Online]. http://cdiac.ornl.gov/ftp/ndp030/CSV-FILES

[2] (2010, May) Jefferson lab. [Online]. http://education.jlab.org/glossary/abund_ele.html

[3] (2010, May) Energy density of hydrogen. [Online]. http://hypertextbook.com/facts/2005/MichelleFung.shtml

[4] (2011, October) Electronic science tutor. [Online]. www.physchem.co.za/OB12-che/electrolysis.htm

[5] Y.H Jeong, M.S Kazimi, K.J Hohnholt, and B Yildiz, Optimization of the hybrid sulfur cycle for hydrogen generation.

[6] Jomard F Feraud and J P Caire, "Numerical modelling of the preliminary design of the hydrogen production electrolyzer in the Westinghouse hybrid cycle," *International journal of hydrogen energy*, vol. 33, pp. 1142-1152, 2008.

[7] (2011, August) [Online]. www.shef.ac.uk/polopoly_fs/1.48209!/file/Westinghouse.doc

[8] William A Summers and John L Steimke, "Development of the hybrid sulfur thermochemical cycle," Savannah River National Laboratory, 2005.

[9] P Sivasubramanian and R Ramasamy, "Electrochemical hydrogen production from thermochemical cycles using a proton exchange membrane electrolyzer," *Journal of hydrogen energy*, vol. 32, pp. 463-468, 2007.

[10] William A Summers and M R Buckner, "Hybrid sulfur thermochemical process development," in *DOE Hydrogen program*, 2005.

[11] (2011, Jun) Electrochemistry encyclopedia. [Online]. http://electrochem.cwru.edu/encycl/art-c02-corrosion.htm

[12] J L Steimke and T J Steeper, "Characterization testing of H2O-SO2 electrolyzer at ambient pressure," 2005.

[13] (2011, May) Fuel cell store. [Online]. http://www.fuelcellstore.com/en/pc/viewPrd.asp?idcategory=155&idproduct=1450

[14] J L Steimke and T J Steeper, "Characterization testing and analysis of a single cell SO2 depolarized electrolyzer," Savanah River National Laboratory, 2006.

[15] S Kalpakjian and S Schmid, *Manufacturing egineering and technology*, 5th ed.: Prentice Hall, 2006.

[16] Xianguo Li and Imran Sabir, "Review of bipolar plates in PEM fuel cells: Flow-field design," *International journal of hydrogen energy*, vol. 30, pp. 359-371, 2005.

[17] Piotr Bujlo, "PEMFC stack components," in *HySA Systems HFCT Training*, Cape Town, 2010.

[18] S Karvonen and T Hottinen, "Modelling of flow field in PEM fuel cell," *Journal of power sources*, vol. 161, pp. 876-884, 2006.

[19] Johannah Itescu, "Polymer electrolyte fuel cells: The gas diffusion layer,".

[20] Hector R Colon-Mercado, Mark C Elvington, and David T Hobbs, "Catalyst characterization for sulfur dioxide depolarized electrolyzer," Savannah River National Laboratory, 2009.

[21] S Maass, F Finsterwalder, G Frank, R Hartmann, and C Merten, "Carbon support oxidation in PEM fuel cell cathodes," 2007.

[22] K Norman, M R Hibbs, J A Staser, J W Weidner, and M A Hickner, "Novel SO2

electrolysis membranes for hydrogen production by the hybrid sulphur thermochemical cycle,".

[23] (2011, October) Electrochemistry encyclopedia. [Online]. http://electrochem.cwru.edu/encycl/art-t01-tafel.htm

[24] Michael F Ashby, *Material selection in mechanical design*, 3rd ed.: Elsevier, 2005.

[25] Bruce R Munson, Donald F Young, and Theodore H Okiishi, *Fundamentals of fluid mechanics*, 5th ed.: Wiley and sons, 2006.

[26] A Levy, "The accuracy of the bubble meter method for gas flow measurements," *Journal of scientific instruments*, vol. 41, pp. 449-453., 1964.

[27] John A Staser and John W Weidner, "Sulfur Dioxide Crossover during the Production of Hydrogen," *Journal of The Electrochemical Society*, 2009.

[28] (2011, September) NiWire Industries. [Online]. http://www.niwire.com/service/technical-data-of-nichrome-80-cold-draw-wire/

[29] (2011, November) Engineers Edge. [Online]. http://www.engineersedge.com/torque.htm

[30] (2011, September) Air Liquide. [Online]. http://encyclopedia.airliquide.com/Encyclopedia.asp?GasID=36

[31] D Hobbs, "Hybrid sulfur electrolyzer component development summary," in *HyS electrolyzer workshop and information exchange*, 2009.

[32] L Steimke J and J Steeper T, "Characterization testing and analysis of single cell SO2 depolarized electrolyzer," Savannah River National Laboratory, 2006.

[33] A Kumar and R G Reddy, "Effect of channel dimensions and shape in the flow-field distributor on the performance of polymer electrolyte membrane fuel cells," University of Alabama, 2002.

[34] Li Xianguo, Sabir Imran, and Park Jaewan, "A flow channel design procedure for PEM fuel cells with effective water removal," University of Waterloo, 2006.

APPENDIX A

Derivation of Material Index for the Back Plate

Using the techniques as discussed in Chapter 3, the following table can be constructed to help find the appropriate back plate material.

Function	Back plate, provide support
Limiting material property	Shear stress (applied torque)
	Maximum operating temperature
Objective	Minimize density
	Maximize thermal conductivity
Free variable	Material

Typical torque values applied to the bolts through the back plate are in the range of 2Nm. This was translated to shear stress of 0.20MPa that the back plate will experience. It is known that the flow field temperature has to be in the range of 80°C, since no materials are specified, a probable temperature that the back plate might reach was subjectively chosen as 200°C.

The values for the shear modulus and maximum operating temperatures were used in the screening step. The design requirements state that the thermal conductivity had to be maximized and the density be minimized. These properties then had to be ranked to find the best suitable material for the function.

The first of the material indices was determined as $M_1=\lambda/\rho$ as is presented in the calculations below.

The heat transfer through the back plate can be given by:

$$Q = \frac{A\lambda\Delta T}{t} \qquad (1)$$

with A- Normal heat transfer area (m^2)

λ- Thermal conductivity of material (W/mK)

ΔT- Temperature difference across back plate (K)

t- Thickness of back plate (m)

The density is given by:

$$\rho = At \quad (2)$$

Combining eq. (1) and (2) by eliminating t will yield:

$$Q = \frac{A^2 \lambda \Delta T}{\rho}$$

Thus the heat flow per unit area of heat transfer can maximized by maximizing λ/ρ, thus M_1= λ/ρ. Taking logarithms on both sides and noting that the equation of a straight line is y=mx+c will show that:

$$\log \lambda = \log \rho + \log M_1$$

From this it can be noted, that the thermal conductivity will have the y-axis position and the density the x-axis position in CES. Thus a line with slope 1 will be used to rank the materials. The line position was then adjusted till only a few materials remained, and material cost was then taken into account in limiting the candidates further. The results for this selection are shown in Table 10.

Table 10: CES results for back plate materials

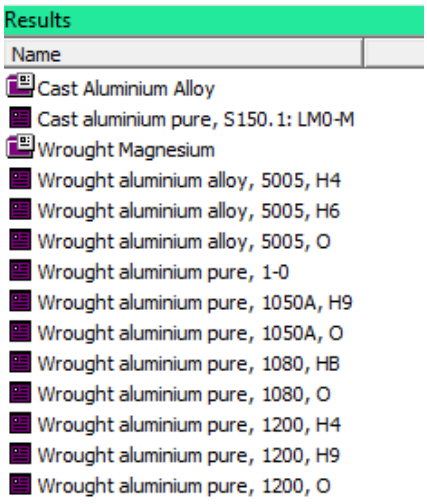

Derivation of Material Index for the Bipolar Plate

Using the techniques as discussed in Chapter 3, the following table can be constructed to help find the appropriate bipolar plate material.

Function	Supply reactants
Limiting material property	Maximum service temperature
	Corrosion resistance
Objective	Minimize cost
	Maximize thermal conductivity
Free variable	Material

The maximum temperature and the materials corrosion resistance against strong acid was used in the screening step. The remaining candidates were then ranked by using the following material index $M_2=\lambda/C_m\rho$ where C_m is the cost of the material per kg.

The index was formulated by noting that:

$$Q = \frac{A\lambda\Delta T}{t} \quad (3)$$

And that

$$C = mC_m = At\rho C_m \quad (4)$$

Eliminating A from eq. (3) and replacing in eq. (4) showed that:

$$C = \frac{Qt\rho C_m}{\Delta T\lambda}$$

Inverting the independent variables will yield the material index as $M_2= \lambda/C_m\rho$. Taking logarithms and noting the equation of a straight line will yield:

$$\log\lambda = \log\rho C_m + \log M_2$$

Thus the thermal conductivity will have the y-axis position, and the product of the material density and the material cost will take the x-axis position in CES. Adjustment of the position of the line with slope 1, until only a few candidates remain yielded the following results:

Table 11: CES results for bipolar plate materials

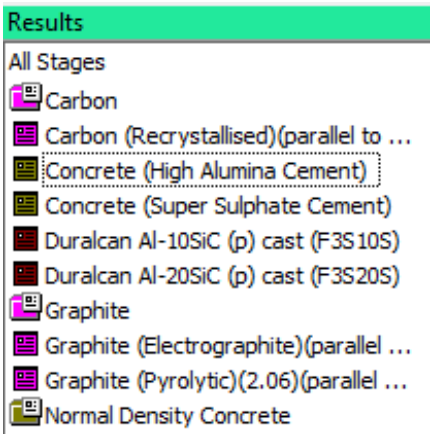

APPENDIX B

EES Calculations of the Pressure Drop through the Flow Channel

The assumptions under which the pressure drop was calculated was already discussed, the program used to determine the pressure drop as a function of the mass flow rate is given by:

```
D_h=(4*A)/O                          "Determining the hydraulic diameter"
b=2.5/1000                           "Width of the channel"
d=3/1000                             "Depth of the channel"
A=d*b                                "Cross sectional area of the channel"
O=2*(d+b)                            "Circumference of the cross section"
V=Q/A
rho=1000                             "Density of water"
g=9.81                               "Gravitaional constant"
l=26*(100/1000)                      "Length of flow channel"
{m_dot=0.15/60}                      "Mass flow rate 150ml/min"
Q=m_dot/rho
Re=(rho*V*D_h)/mu
mu=1.12e-3                           "Viscosity of water"
h_l_90=h_l_major + h_l_minor_90
h_l_U=h_l_major + h_l_minor_U
h_l_major=(f*l*V^2)/(D_h*2*g)
f=64/Re                              "Friction factor"
h_l_minor_90=(K_l_90*V^2)/(2*g)
h_l_minor_U=(K_l_U*V^2)/(2*g)
K_l_90=(2*0.3)*50                    "K_l=2*0.3 for 90 degree elbows and
0.2 for U-bends"
K_l_U=0.2*50

DELTAp_90=(rho*g*h_l_90)/1000        "Pressure drop when using 90 dgree
elbows"
DELTAp_U=(rho*g*h_l_U)/1000          "Pressure drop when using U-bends"
```

Results Obtained from EES

Table 12: Results for the pressure drop through the flow channel

Parametric Table

Table 2

1..10	1 ṁ	2 Δp_{90}	3 Δp_U
Run 1	0.001	1.937	1.759
Run 2	0.002	4.407	3.696
Run 3	0.003	7.411	5.811
Run 4	0.004	10.95	8.104
Run 5	0.005	15.02	10.57
Run 6	0.006	19.62	13.22
Run 7	0.007	24.76	16.05
Run 8	0.008	30.43	19.05
Run 9	0.009	36.63	22.23
Run 10	0.01	43.37	25.59

ANSYS Simulation of Internal Pressure Distribution

The analysis was done by using ANSYS along with its Mechanical solver. The analysis was done by creating a sub assembly consisting of the back plate and the bipolar plate, with the pressure applied to all the faces within the flow channels, including the inlet and outlet areas along with the port holes. The reason for this is that failure will occur in the bipolar plate rather than the current collector or electrical insulation, and the back plate provides the bipolar plate with the necessary support.

The mechanical properties for the analysis on the back plate and bipolar plate were obtained from CES. The lowest strength values were used since this will provide the most conservative result.

APPENDIX C

Heating Element Design

From the fundamentals of heat transfer the power required by the heat source for steady state, one dimensional heat transfer is given by:

$$q = \frac{\Delta T}{\sum R_t} \quad (5)$$

with q- Power required (W)

ΔT - Temperature difference that q has to facilitate (K)

ΣR_t- Sum of the thermal resistances over ΔT (W/K)

The thermal resistance of a material against conduction can be defined as:

$$R = \frac{L}{kA} \quad (6)$$

with L- The length of material over which q is to be transferred (m)

k- Thermal conductivity of the material (W/mK)

A- Area normal to the direction of heat transfer (m^2)

In the case of convection, the thermal resistance is given by:

$$R = \frac{1}{hA} \quad (7)$$

with h- The convection heat transfer coefficient

A- Area normal to the direction of heat transfer

Since the electrolyzer is not perfectly insulated, the heat from the heat source will conduct in the x and –x direction, that is, towards the flow field and away from it. Thus the total power required will have two components so that:

$$q = q_x + q_{-x}$$

By using eq. (6) and (7) in calculating the thermal resistances of the materials in the electrolyzer and substituting into eq. (5), q_x and q_{-x} may be determined, thus giving the total power required by the heat source.

Calculations were done using EES under the following assumptions:

- Outer edges are adiabatic.
- Convection was only considered on the heat pad side and radiation was neglected due to expected relative low impact.
- Assume steady state conditions.
- AL45 heat insulation will be placed on the outer edges of the heating pad.

EES Calculations to Determine the Heat Distribution through the Electrolyzer

"Thermal conductivities of the various materials"

```
k_air=26.3e-3
k_heat_insulation=1
k_backplate=180
k_silicone=0.38
k_copper=290
k_graphite=110
```

"Thicknesses of the various materials"

```
L_heat_insulation=25/1000
L_backplate=10/1000
L_silicone=1.5/1000
L_copper=0.7/1000
L_graphite=10/1000
```

"Surface area exposed to heat source of the various materials"

```
A_element=(150/1000)*(150/1000)
A_graphite=A_element
A_silicone=(200/1000)*(200/1000)
A_copper=A_element
A_backplate=A_silicone
A_heat_insulation=A_silicone
```

"Calculations of the thermal resistance of the various materials"

"Calculations for determining the convection heat transfer coefficient"

```
Re=(V*L)/nu
V=0.5
L=150/1000
nu=15.89e-6

Pr=nu/alpha
alpha=22.5e-6

Nus_x=0.664*Re^(1/2)*Pr^(1/3)
Nus_x=(h_x*L)/k_air

R_air=1/(h_x*A_heat_insulation)
R_heat_insulation=L_heat_insulation/(k_heat_insulation*A_heat_insulation)
R_backplate=L_backplate/(k_backplate*A_backplate)
R_silicone=L_silicone/(k_silicone*A_silicone)
R_copper=L_copper/(k_copper*A_copper)
R_graphite=L_graphite/(k_graphite*A_graphite)
```

```
R_t=R_air+R_heat_insulation+R_backplate+R_silicone+R_copper+R_graphite

"The power output of the heating element was varied in a parametric table in order to see what the required
power will have to be so that the flow field temperature will be 80C"

"Assumptions:                                    Ambient temperature is 25C
                                                 Electrolyzer is perfect insulated at
the edges
                                                 The power is focused on one point
                                                 and flows through the electrolyzer"

T_ambient=25+273
T[1]=T_ambient

q=(T[3]-T[1])/(R_heat_insulation+R_air)+(T[3]-
T_ambient)/(2*(R_backplate+R_silicone+R_copper+R_graphite)+R_air)
{q=45}
q=(T[3]-T[2])/R_heat_insulation
q=(T[3]-T[4])/R_backplate
q=(T[4]-T[5])/R_silicone
q=(T[5]-T[6])/R_copper
q=(T[6]-T[7])/R_graphite
q=(T[7]-T[8])/R_graphite
q=(T[8]-T[9])/R_copper
q=(T[9]-T[10])/R_silicone
q=(T[10]-T[11])/R_backplate
q=(T[11]-T[12])/R_heat_insulation

"To compensate for the assumptions above, a safety factor needs to be in place"
SF=2
q_SF=SF*q
```

EES returned the power required by the heating pad to get the flow fields to a temperature of 100ºC as 40W. The temperature distribution with a 40W heating pad through the cell can be seen in the Figure 57 and was also calculated using the above program.

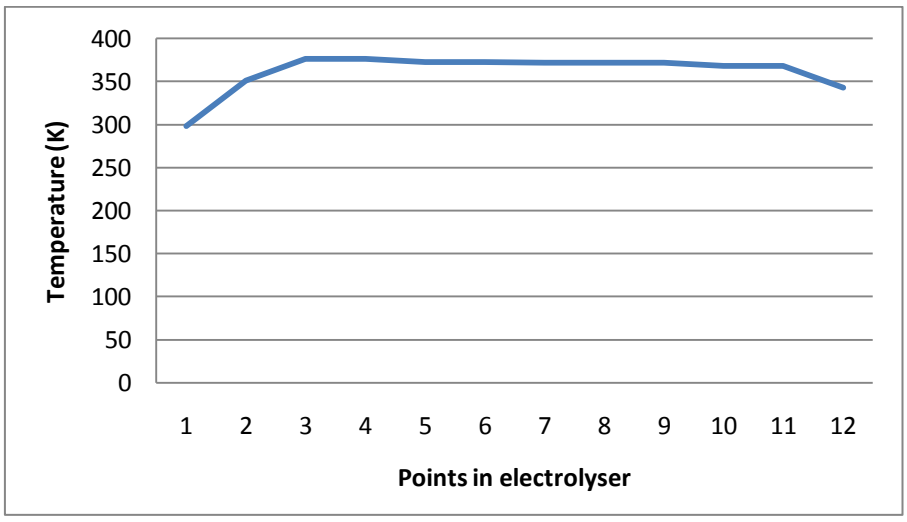

Figure 57: Temperature distribution through electrolyzer

The electrolyzer points indicated in Figure 57 are clearly presented in Figure 58 and Table 13

Table 13: Indication of the position in the electrolyzer

Point in Figure 57	Position in electrolyzer assembly
1	Ambient air (25ºC)
2	Layer between ambient air and heat insulation
3	Layer between heat insulation and back plate
4	Layer between heat insulation and silicone
5	Layer between silicone and copper plate
6	Layer between copper plate and 1st graphite flow field
7	Layer between graphite flow fields
8	Layer between copper plate and 2nd graphite flow field
9	Layer between silicone and copper plate
10	Layer between heat insulation and silicone
11	Layer between heat insulation and back plate
12	Layer between ambient air and heat insulation

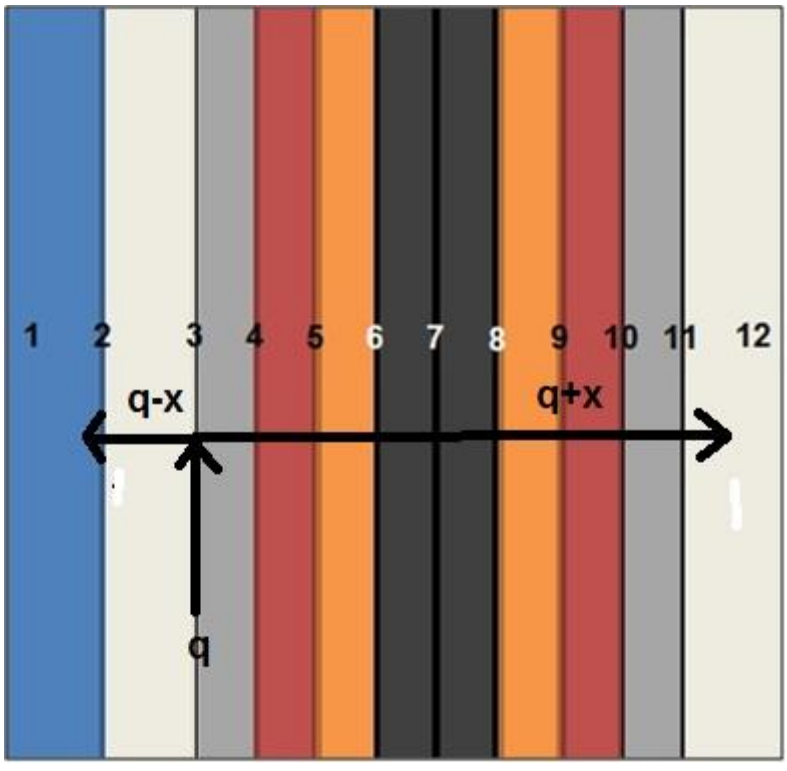

Figure 58: Figure indicating the positions in electrolyzer

In determining q, a couple of assumptions were made, the most important one being top and bottom edges of the cell were adiabatic surfaces and that the process is a steady state process. To compensate for this heat loss through the adiabatic surfaces and the material in which the heating element will be contained, a safety factor of 1.5 was subjectively chosen. Thus the final power required by the heat pad will be 60W.

In constructing the heat pad, it should be noted that the relay that will be used to control the temperatures makes use of a 230V power supply. Ohm's law states that:

$$P = VI$$

With P- Power required by heat pad (W)

V- Voltage applied to facilitate P

I- Induced current due to applied voltage (A)

Thus a current of 0.26A will be induced in the heating element. Taking this information and noting a different form of Ohm's law, the electrical resistance of the heating element may be calculated:

$$V = IR$$

With R- Electrical resistance (Ω)

The resistance that the heating pad element should posses is 881.67Ω, this is under the assumption that the temperature resistance factor may be discarded because of the relatively low operating temperatures. Since materials electrical resistivity is given in terms of Ω/m, the length of the heating element should be known.

To determine the length of the element, it was assumed that the electrical resistive wire, forming the element, will conform to the flow channel geometry along with a section for the connectivity to the power supply. The length of the wire was determined as ±2.7m using SolidWorks, resulting in a resistance per unit length of 326.5Ω/m.

The next step in the design was to locate a wire with a resistance of 326.5Ω/m. Since NiChrome wires are the most common heating element material, the search was started there. The closest value to that required was from a 0.07mm NiChrome 80 cold drawn wire, it had a resistance of 287Ω/m [29]. This however means that the length of the wire will have to be corrected, the corrected length was calculated as 3.14m. This excess length can be equally distributed over the bipolar plate surface area.

APPENDIX D

Safety Considerations

A short oversight of MSDS of the various reactants and products are discussed in this section. The student had to be familiar with the safety aspects concerned to prevent harm to him or any other bystanders.

Sulphuric Acid

Sulphuric acid is odourless substance, it would be wise to perform the experiments in a well ventilated room to prevent the risk of gas inhalation. The acid is a strong corrosive and will react with any combustibles or reducing agents and organic materials. Sulphur oxides, which are toxic, may be formed if sulphuric acid is significantly heated. The exposure to various concentrations of sulphuric acid along with the associated health risks are shown in the table below:

Concentration	Health Effects
<1.0mg/m^3	No acute effects expected
1.0-2.0 mg/m^3	Eye, nose and throat irritation expected
2.0-5.0 mg/m^3	Severe eye, nose and throat irritation, burning sensation, cough, shortness of breath
>5mg/m^3	Inhalation may result in pulmonary edema. Symptoms may only appear after a few hours. Medical observation is needed
15mg/m^3	Immediately dangerous to life and health

Table 14: Concentration level of sulphuric acid vs. health effects

When working with liquid sulphuric acid, splash proof face protection should be worn at all times. Gloves should preferably be made from PVC or some

other chemical resistant substance. Water should never be poured into the acid when diluting, may cause significant heat generation. Always add the acid to the water, this should be done slowly and in a glass container.

Sulphur Dioxide

Sulphur dioxide is a highly irritating gas to the eyes and throat and can cause respiratory reflexes. Liquid sulphur dioxide may cause tissue burns. When mixed with water, sulphur dioxide becomes very corrosive. The substance should only be handled in a well ventilated area. Splash proof eye-wear and chemically resistant gloves should be worn when being handled. The acid is non-flammable or explosive and requires extreme temperatures to decompose.

Hydrogen

Hydrogen is colourless, odourless gas, at room temperature, that is essentially non-toxic. When inhaled, without adequate flow of oxygen to the lungs, it may cause dizziness and nausea. It is advisable that persons with ill health not work with the gas since it may aggravate the illness. Since hydrogen is very flammable in a wide range of air mixtures, ensure there are no open flames present. Work should be conducted in a well ventilated room.

APPENDIX E

Compression Tests on Hypalon Gasket

The compression tests were done by applying a compression force to a square section of the Hypalon sheet and noting the deflection of the sheet. The compression force, associated with the desired deflection, was then converted to a torque that has to be applied to each bolt on the electrolyzer. The force-torque relation is given by [29]:

$$T = 0.2DF$$

with T - Applied torque (inch.pounds)
D - Nominal bolt diameter (inch)
F - Bolt force (pounds)

Figure 59: Compression test, test bench

The maximum protrusion height of the flow fields that could be achieved was 1.2mm due to the geometry of the already manufactured part. The protrusions and the MEA had a total thickness of 1.5mm. Thus both gaskets had to deform 0.3mm to provide an adequate seal between the bipolar plates.

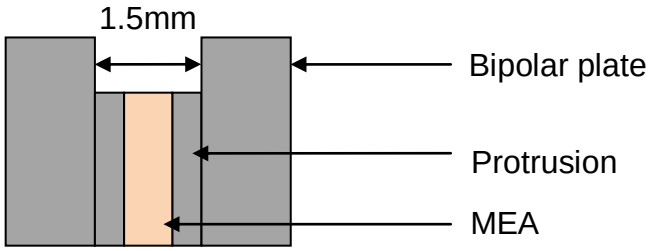

The compressions tests were then conducted and showed that the average force necessary to deflect the gasket 0.3mm was in the region of 0.5kN (see Figure 60). This was then converted to torque that needs be applied to each bolt in the SDE assembly. The force was converted to a 4Nm torque that has to be applied to each bolt in the back plates. The gasket was then cut using a laser cutter to ensure good dimensional accuracies.

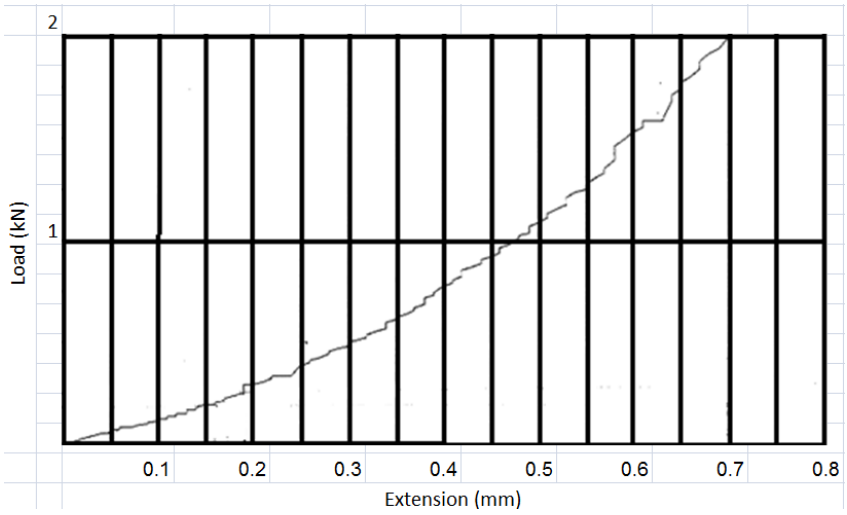

Figure 60: Load-deformation curve of compression test result

APPENDIX F

Calculation of Electrolyzer Efficiency

The electrolyzer efficiency was determined by only considering the energy contained within the hydrogen gas and the heat and electrical input required for electrolysis. The equation in determining the efficiency was as follows:

$$\eta = \frac{energy\ contained\ in\ H_2}{heat\ energy + electrical\ energy}$$

The energy contained in the hydrogen gas was calculated by using the rate of hydrogen gas produced and assuming a gas density of 0.085 kg/m^3 (atmospheric conditions) and the energy value of the gas was 143 MJ/kg [29].

The heat energy input will be 60W, as calculated in Chapter 3, although a 750W heat pad will be used to save on the experimental run time. The 25cm^2 scale cell is already equipped with a 40W heat pad to supply the sufficient temperature.

The electrical energy term is governed by ohms law, which can be stated as:

$$P = VI$$

With V- Induced cell potential (V, measured during testing)
I- Applied current (A, measured during testing)
P- Electrical energy input (W)

APPENDIX G

Manufacturing drawings

List of drawings		
Component	**Material**	**Drawing number**
Back plate	UNS 5005 Al alloy	SDEBP1
Current collector	C12220	SDECC1
Electrical insulation	Eccosil	SDEEI1
Bipolar plate	Phenolic resin impregnated graphite	SDEFF1 and SDEFF2
Inlet/Outlet	PTFE	SDEIO1
Leakage tray[8]	Perspex	SDELT1

[8] Dimensions are not indicated since the laser cutter makes of a 1:2 scale drawing and no dimensions are necessary

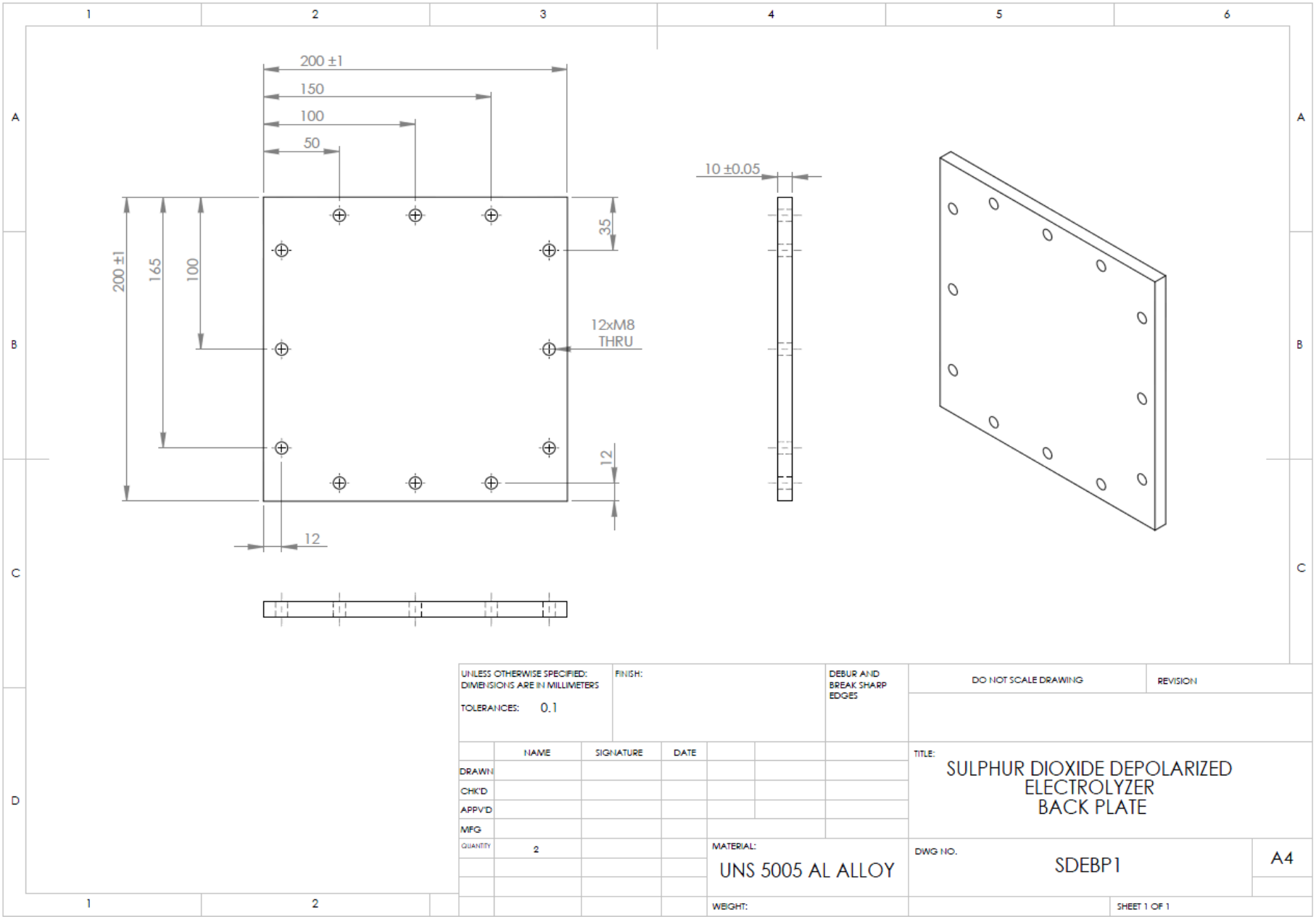

UNLESS OTHERWISE SPECIFIED: DIMENSIONS ARE IN MILLIMETERS TOLERANCES: 0.1	FINISH:		DEBUR AND BREAK SHARP EDGES		DO NOT SCALE DRAWING	REVISION
	NAME	SIGNATURE	DATE		TITLE: SULPHUR DIOXIDE DEPOLARIZED ELECTROLYZER BACK PLATE	
DRAWN						
CHK'D						
APPV'D						
MFG						
QUANTITY	2			MATERIAL: UNS 5005 AL ALLOY	DWG NO. SDEBP1	A4
				WEIGHT:		SHEET 1 OF 1

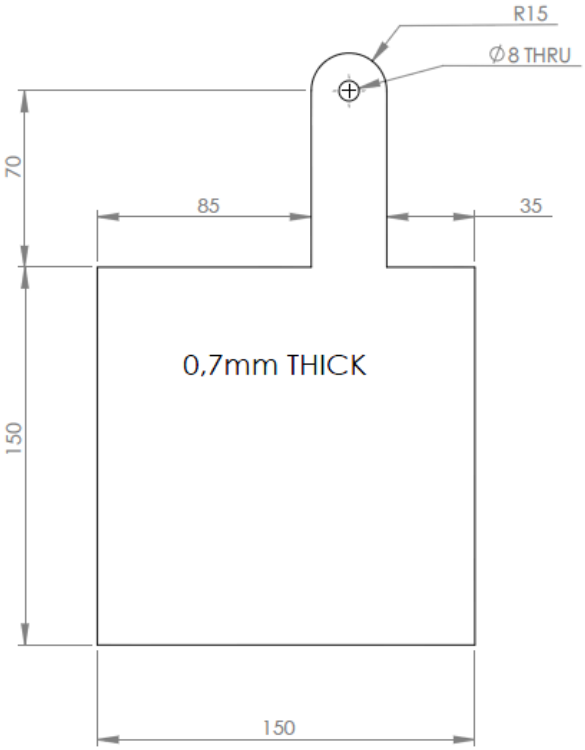

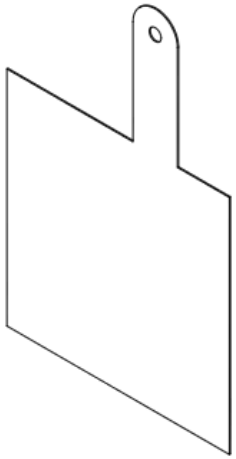

UNLESS OTHERWISE SPECIFIED: DIMENSIONS ARE IN MILLIMETERS TOLERANCES: 0.1		FINISH:		DEBUR AND BREAK SHARP EDGES		DO NOT SCALE DRAWING	REVISION
	NAME	SIGNATURE	DATE			TITLE: SULPHUR DIOXIDE DEPOLARIZED ELECTROLYZER CURRENT COLLECTOR	
DRAWN							
CHK'D							
APPV'D							
MFG							
QUANTITY	2			MATERIAL: UNS C12220 CU ALLOY		DWG NO. SDECC1	A4
				WEIGHT:		SHEET 1 OF 1	

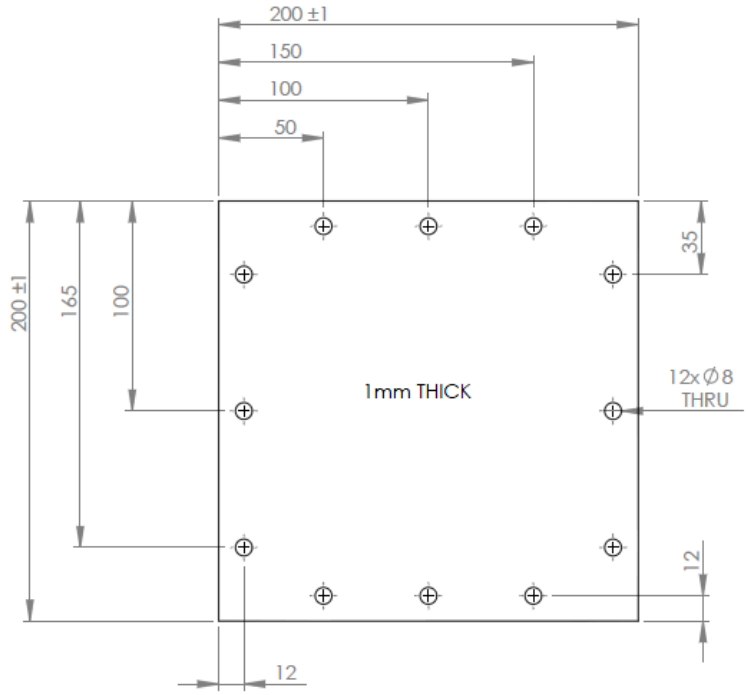

UNLESS OTHERWISE SPECIFIED: DIMENSIONS ARE IN MILLIMETERS TOLERANCES: 1	FINISH:		DEBUR AND BREAK SHARP EDGES		DO NOT SCALE DRAWING	REVISION
	NAME	SIGNATURE	DATE		TITLE: SULPHUR DIOXIDE DEPOLARIZED ELECTROLYZER ELECTRICAL INSULATION	
DRAWN						
CHK'D						
APPV'D						
MFG						
Q.A				MATERIAL: SILICONE ELASTOMER	DWG NO. SDEEI1	A4
				WEIGHT:		SHEET 1 OF 1

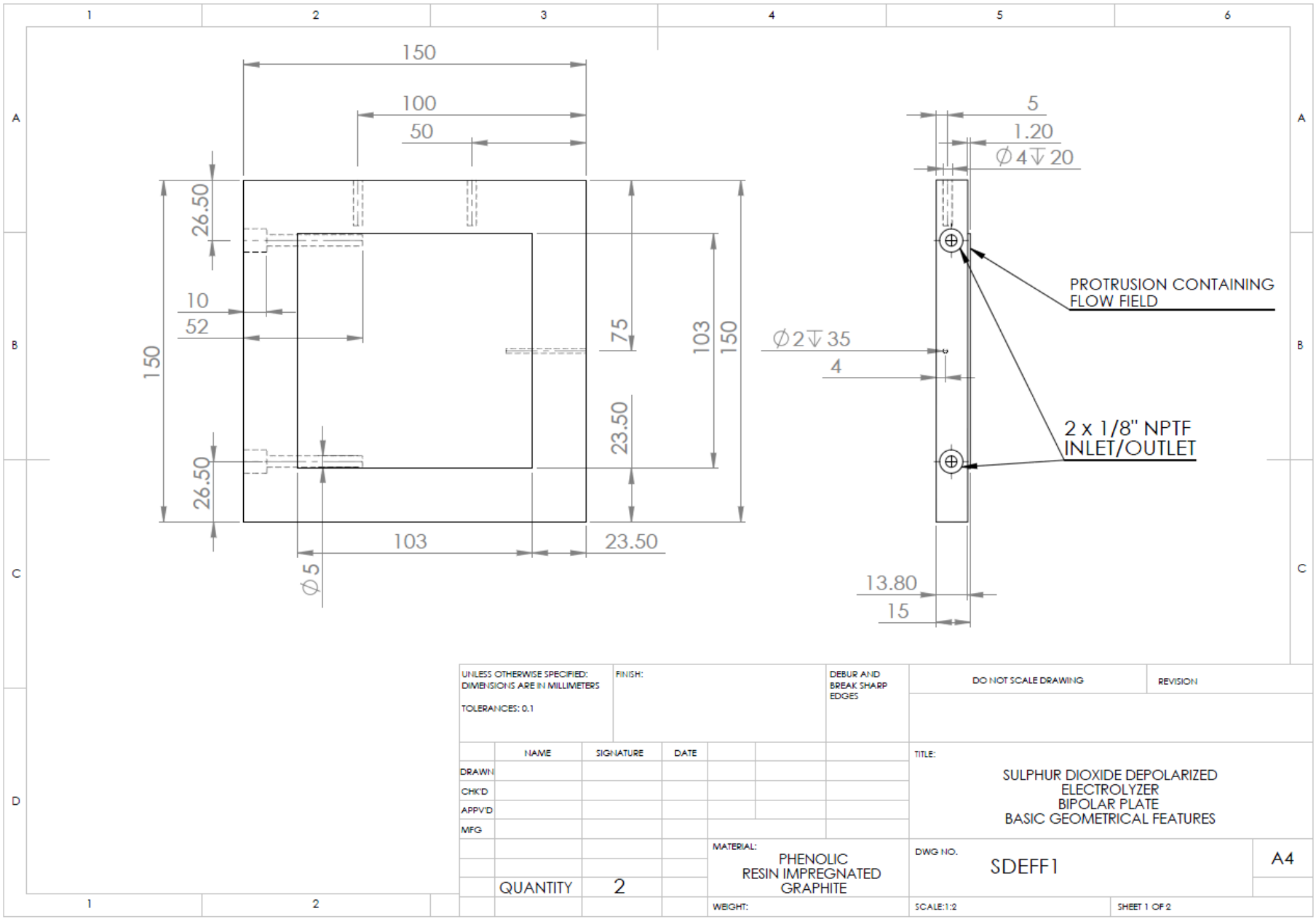

UNLESS OTHERWISE SPECIFIED: DIMENSIONS ARE IN MILLIMETERS TOLERANCES: 0.1	FINISH:	DEBUR AND BREAK SHARP EDGES	DO NOT SCALE DRAWING	REVISION	
	NAME	SIGNATURE	DATE	TITLE: SULPHUR DIOXIDE DEPOLARIZED ELECTROLYZER BIPOLAR PLATE BASIC GEOMETRICAL FEATURES	
DRAWN					
CHK'D					
APPV'D					
MFG					
QUANTITY	2	MATERIAL: PHENOLIC RESIN IMPREGNATED GRAPHITE		DWG NO. SDEFF1	A4
		WEIGHT:		SCALE:1:2	SHEET 1 OF 2

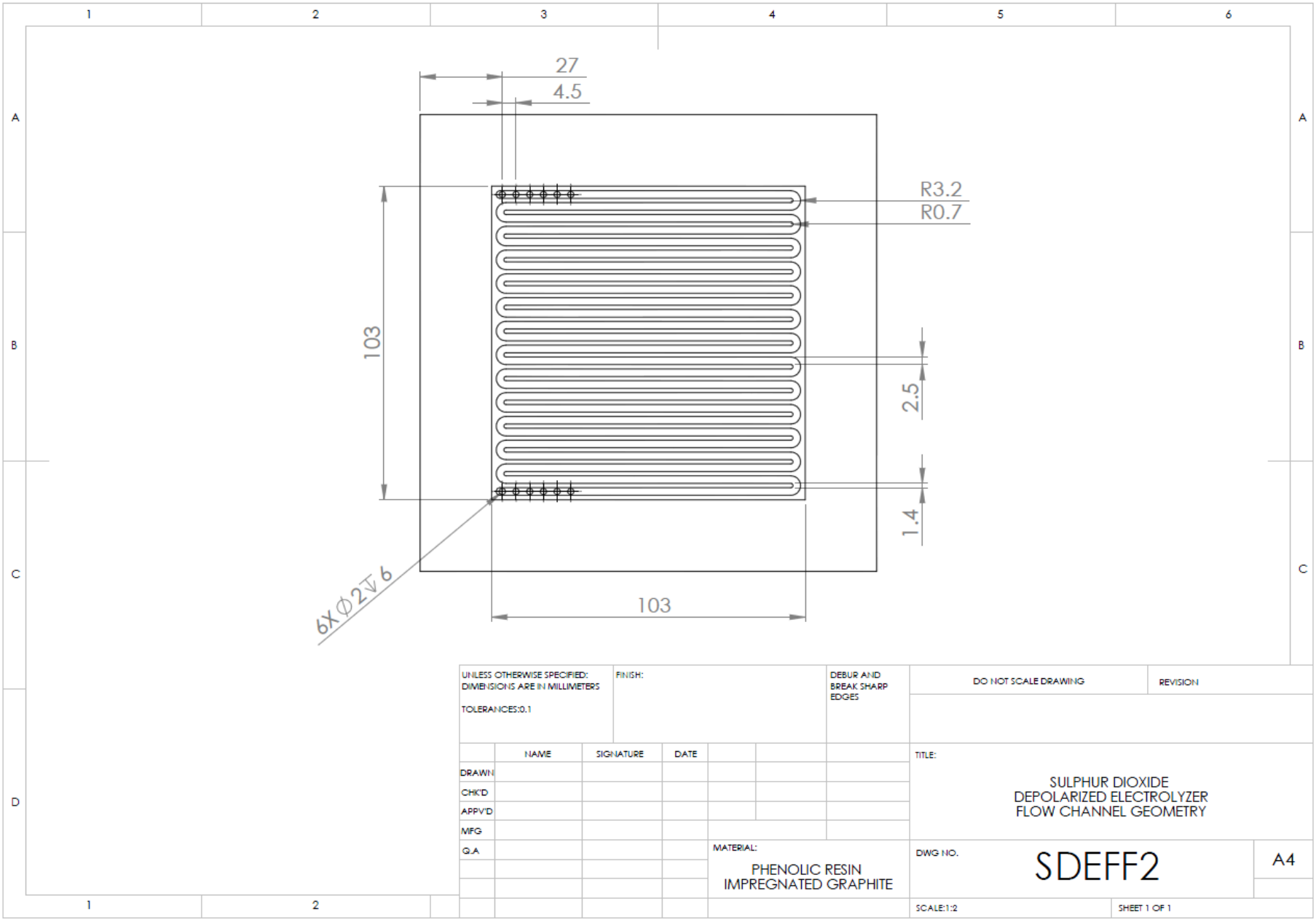

UNLESS OTHERWISE SPECIFIED: DIMENSIONS ARE IN MILLIMETERS TOLERANCES:0.1	FINISH:		DEBUR AND BREAK SHARP EDGES		DO NOT SCALE DRAWING	REVISION
	NAME	SIGNATURE	DATE		TITLE: SULPHUR DIOXIDE DEPOLARIZED ELECTROLYZER FLOW CHANNEL GEOMETRY	
DRAWN						
CHK'D						
APPV'D						
MFG						
Q.A				MATERIAL: PHENOLIC RESIN IMPREGNATED GRAPHITE	DWG NO. SDEFF2	A4
					SCALE:1:2	SHEET 1 OF 1

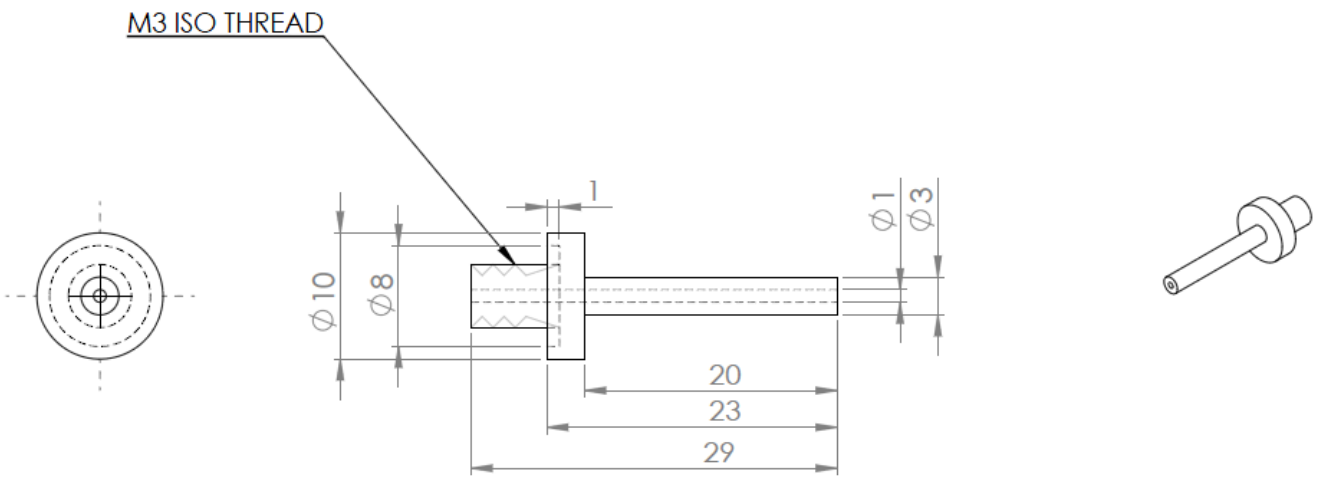

UNLESS OTHERWISE SPECIFIED: DIMENSIONS ARE IN MILLIMETERS TOLERANCES: 0.1	FINISH:	DEBUR AND BREAK SHARP EDGES	DO NOT SCALE DRAWING	REVISION	
	NAME	SIGNATURE	DATE	TITLE: SULPHUR DIOXIDE DEPOLARIZED ELECTROLYSER INLET/OUTLET	
DRAWN					
CHK'D					
APPV'D					
MFG					
QUANTITY	6			MATERIAL: PTFE	DWG NO. SDEIO1 A4
				WEIGHT:	SCALE:2:1 SHEET 1 OF 1

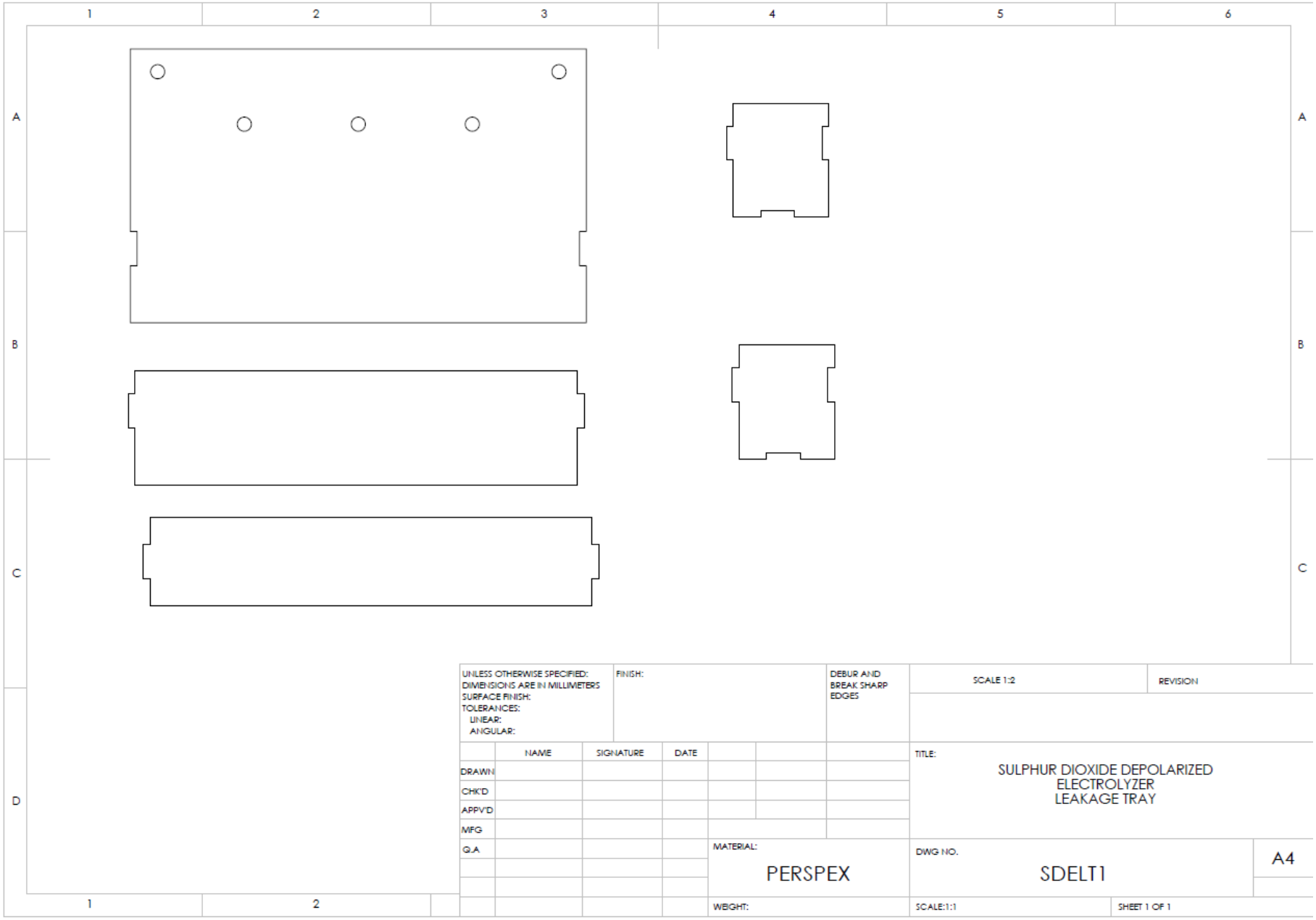
1
2
3
4
5
6
A
B
C
D
UNLESS OTHERWISE SPECIFIED:
DIMENSIONS ARE IN MILLIMETERS
SURFACE FINISH:
TOLERANCES:
LINEAR:
ANGULAR:
FINISH:
DEBUR AND BREAK SHARP EDGES
SCALE 1:2
REVISION
NAME
SIGNATURE
DATE
DRAWN
CHK'D
APPV'D
MFG
Q.A
TITLE:
SULPHUR DIOXIDE DEPOLARIZED ELECTROLYZER LEAKAGE TRAY
MATERIAL:
PERSPEX
DWG NO.
SDELT1
A4
WEIGHT:
SCALE:1:1
SHEET 1 OF 1